Superhard diamondlike carbon: preparation, theory, and properties

Q. Wei and J. Narayan

One of the many forms of carbon, diamondlike carbon (DLC) or tetrahedral amorphous carbon (ta-C) consists mainly of sp^3 bonded carbon atoms. If properly prepared, DLC can have properties that rival those of crystalline diamond. The beneficial properties of DLC stem from the continuous rigid random networks of sp^3 carbon atoms, and the properties can essentially be tailored by controlling the sp^3/sp^2 ratio. Techniques that have been successfully used to prepare high quality DLC coatings or thin films include pulsed laser ablation, filtered cathodic vacuum arc deposition, and mass selected ion beam deposition. Diamondlike carbon coatings that possess properties close to diamond in terms of hardness, atomic smoothness, infrared transparency, and chemical inertness can be processed easily with these techniques. In the past decade, tremendous progress has been made in experimental and theoretical investigations of hydrogen free DLC. Experimental and commercial applications in areas including microelectronics, microtribology, and biomedical technologies have been demonstrated. Potential applications include sensors, flat panel displays (field emitters), and photodiodes. Past and recent developments in synthesis and processing, properties, and modelling of hydrogen free superhard amorphous DLC are comprehensively reviewed. The techniques of fabrication, theoretical modelling, physical and mechanical characterisation, properties, and present and potential applications of DLC are discussed. IMR/357

Dr Wei is in the NSF Centre for Advanced Materials and Smart Structures, Department of Mechanical Engineering, North Carolina A&T State University, Greensboro, NC 27411, USA (email quiming@ncat.edu) and Professor Narayan is in the Department of Materials Science and Engineering, North Carolina State University, Raleigh, NC 27695–7916, USA.

Introduction

Carbon, the sixth member of the periodical table, has turned out to be one of the most fascinating elements in nature.[1] Its crystalline polytypes are well known, namely the diamond or zinc blende structure, the layered graphite structure, and the puckered hexagonal diamond, or lonesdite.[2] More recently, fullerene[3] (C_{60}) and nanotubes have created tremendous scientific interest.[4,5] The nanotubes are predicted to be either metallic or semiconducting depending upon their diameter and the helicity of the arrangement of graphitic rings in their walls. Because of their strong in plane bonding, the graphitic sheets are predicted to have higher bulk modulus than diamond. Using a semiempirical approach, bulk modulus B (GPa) for tetrahedrally bonded phases such as diamond can be expressed as $B = (N_C/4)(1972 - 220I)/d^{3.5}$, where N_C is the coordination number and d (Å) is the bond length.[6] The ionicity parameter I accounts for the charge transfer. Since $d = 1{\cdot}54$ Å in diamond compared with the carbon–carbon bond length of 1·42 Å in graphitic sheet, nanotubes and C_{60} are expected to have higher bulk modulus and stiffness than diamond.[7]

Diamondlike carbon (DLC) is an amorphous form of carbon with a large fraction of sp^3 bonds. First experiments to synthesise DLC involved chemical vapour deposition from methane at low temperatures. The resulting DLC films contained a large fraction of hydrogen. It was believed that hydrogen is necessary to stabilise DLC and correlations between sp^3 fraction and hydrogen content were developed. However, in 1989, the formation of high quality DLC films by pulsed laser ablation of carbon clearly demonstrated that hydrogen is not necessary for the stability of sp^3 bonds. Thus, the concept of hydrogen free DLC was clearly established.[8]

The great variety of structures and properties exhibited by carbon stems from its unique chemistry. The ground state configuration of carbon is $2s^2 2p_x^1 2p_y^1$, which suggests that a carbon atom should be capable of forming only two bonds. The tetravalence of carbon is achieved by allowing for promotion, i.e. the excitation of an electron to an orbital of higher energy. Although electron promotion requires an investment of energy, it is worthwhile if that energy can be more than recovered in the greater strength or number of bonds that it allows to be formed. In carbon, the promotion of a 2s electron to a 2p orbital leads to the configuration $2s^1 2p_x^1 2p_y^1 2p_z^1$, with four unpaired electrons in separate orbitals. These electrons may pair with four electrons in orbitals provided by four other atoms and hence form four electron pair σ bonds. The formation of four bonds is a characteristic feature of carbon because the promotion energy is quite small: the promoted electron leaves a doubly occupied 2s orbital and enters a vacant 2p orbital, hence significantly relieving the electron–electron repulsion experienced in the former.[9]

The concept of hybrid orbitals has to be invoked to give a more complete description of the process of bond formation with the promoted state of carbon. It is understood that the electron density distribution in the excited atom is equivalent to the electron density in which each electron occupies a hybrid orbital formed by the interference between the C 2s and C 2p orbitals. The specific linear combinations that give rise to four equivalent hybrid orbitals are termed sp^3 hybrid orbitals

$$\left.\begin{aligned} h_1 &= s + p_x + p_y + p_z \\ h_2 &= s - p_x - p_y + p_z \\ h_3 &= s - p_x + p_y - p_z \\ h_4 &= s + p_x - p_y - p_z \end{aligned}\right\} \quad \ldots\ldots\ldots (1)$$

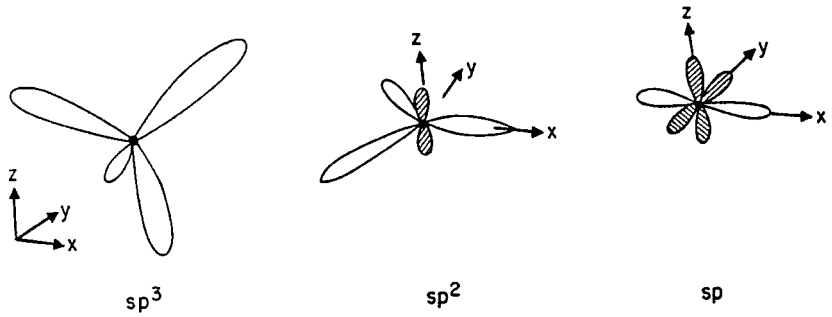

1 Schematic illustration of the three possible hybridisations of carbon[9]

These four sp^3 orbitals can, for example, form four σ bonds with four H atoms to produce a CH_4 (methane) molecule.

Likewise, instead of using four orbitals to form hybrids, we can form sp^2 hybrid orbitals by superposition of an s orbital and two p orbitals

$$\left.\begin{aligned} h_1 &= s + 2^{1/2}p_y \\ h_2 &= s + (\tfrac{3}{2})^{1/2}p_x - (\tfrac{1}{2})^{1/2}p_y \\ h_3 &= s - (\tfrac{3}{2})^{1/2}p_x - (\tfrac{1}{2})^{1/2}p_y \end{aligned}\right\} \quad \ldots\ldots (2)$$

which can form C_2H_4 (ethane) molecules, for example. A similar description applies to the linear acetylene molecule H–C≡C–H, but now the C atoms are sp hybridised and the σ bonds are formed by using hybrid atomic orbitals of the form

$$\left.\begin{aligned} h_1 &= s + p_z \\ h_2 &= s - p_z \end{aligned}\right\} \quad \ldots\ldots\ldots\ldots (3)$$

The three types of hybridisation are schematically illustrated in Fig. 1.[9] In the case of diamond, all the carbon atoms form σ bonds with the four sp^3 hybrid orbitals. Graphite uses the sp^2 hybridisation to form a trigonal plane consisting of three σ bonds, and the remaining p_z orbital forms a relatively weak π bond that is perpendicular to the triangle. This configuration makes graphite a layered structure that can be used as a good lubricant. Here we see the great diversity of carbon properties arising from differences in bonding state and atomic structure: while one of the two structures has been considered to be the hardest known material, its counterpart has been widely used as a good lubricant.

Approximately a decade ago, several reviews were published, mainly owing to Robertson, on the structure, physical and chemical properties, mechanical behaviour and preparation of DLC.[10–12] At that time, most of the reported DLC films were hydrogenated, and the preparation methods were traditional vapour deposition processes that are thermodynamically close to equilibrium. The hydrogen is envisaged to affect adversely both stability and hardness of the DLC films. The past decade has witnessed tremendous interest and ever growing effort in the study of almost every aspect of DLC. Topics studied include the utilisation of novel and innovative thin film processes to produce hydrogen free, dense, high quality DLC films; experimental studies on the electronic properties, atomic structure, and mechanical properties; and extensive theoretical modelling. Several international conferences and workshops have been organised with the focus on the preparation, properties, theory, and applications of DLC, the latest including the MRS symposiums held in Boston in 1997, an international conference dedicated to the state of the art of amorphous carbon,[13] and an MRS symposium in 1999. It is thus an appropriate time to review the developments in this important area over the past decade.

The present review will focus on the preparation, microstructure, atomic structure, characterisation, and applications of hydrogen free DLC films.

Preparation of DLC

The diamondlike phase or sp^3 bonded carbon is a thermodynamically metastable phase, since free energy of formation of diamond at 300 K is 394·5 kJ mol^{-1}, compared with 391·7 kJ mol^{-1} for graphite.[14] These two phases of carbon both have a rather large activation barrier, although the difference in free energy is only 2·8 kJ mol^{-1}. This relative free energy of formation also suggests that the difficulty in converting graphite into diamond is the result of a large activation barrier. Thus the formation of DLC films requires non-equilibrium processing in order to obtain metastable sp^3 bonded carbon. Equilibrium processing methods such as electron beam evaporation of graphite or carbon, where the average energy of the evaporated species is close to kT, lead to formation of 100% sp^2 bonded carbon. The chemical vapour deposition (CVD) methods are also equilibrium methods; however, the presence of atomic hydrogen during CVD processing helps to stabilise sp^3 bonds. From experience of CVD processing with hydrogen bearing carbon compounds, many authors had hypothesised that the presence of hydrogen is a necessary condition for the formation of sp^3 bonds in DLC films.

A major breakthrough in the synthesis of DLC films came with pulsed laser deposition (PLD) of hydrogen free DLC films. The PLD experiments clearly demonstrated that the presence of hydrogen is not necessary for the formation of sp^3 bonds. Highly energetic photons from the pulsed laser beams excite sp^2 bonded carbon atoms into a C* (excited carbon) state and these excited carbon atoms subsequently cluster to form DLC films as follows

$$C\,(sp^2\ \text{bonded}) + h\nu \rightarrow C^*$$

$$C^* + C^* \rightarrow (sp^3\ \text{bonded})$$

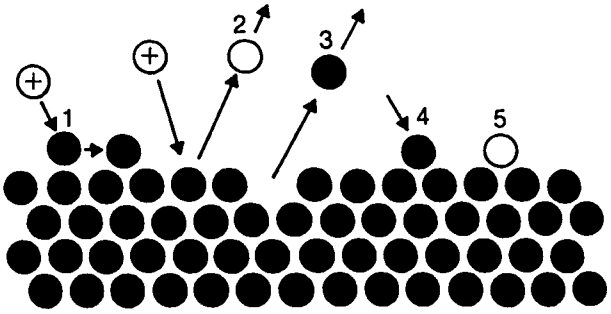

1 impinging ion providing energy for lateral motion of surface atom into advantageous site; 2 sputtering of impurity gas atom from surface; 3 sputtering of loosely bonded solid atom from surface; 4 solid atom or ion depositing on surface; 5 gas atom contaminating surface

2 Illustration of principles of direct ion beam deposition,[22] showing effects of energetic ion flux on surface atoms

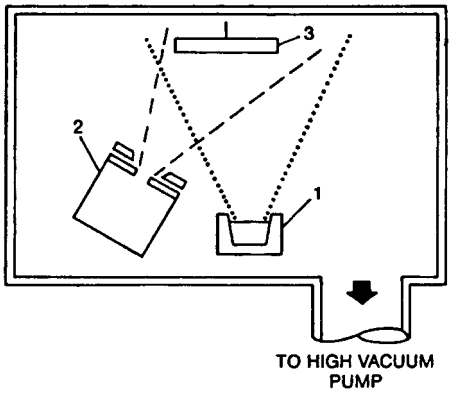

1 evaporative source of deposited material; 2 ion source; 3 substrate

3 Schematic illustration of system for ion assisted deposition[22]

Therefore, the DLC synthesis and processing methods can be divided into two groups: chemical vapour deposition (CVD) and physical vapour deposition (PVD) methods involving carbon bearing compounds; and PVD methods based on energetic ablation of carbon. The first group includes ion beam assisted CVD deposition,[15] plasma enhanced deposition using a dc glow discharge from hydrocarbon gas,[16] plasma deposition using an rf glow discharge from a hydrocarbon gas,[17] microwave discharge,[18] and so on. The second includes cathodic arc deposition,[19] sputtering of carbon targets (graphite),[20] mass selected ion beam deposition,[21] pulsed laser ablation (PLA),[8] and so forth.

In the sections that follow, brief descriptions and comparisons will be presented for the techniques that have been widely employed to prepare hydrogen free DLC films.

Ion beam deposition of DLC films

The first ion beam apparatus used to produce DLC films was due to Aisenberg;[15] this generated carbon ions by sputtering carbon electrodes in an argon plasma. A detailed review on the ion beam and ion assisted deposition of DLC films was given by Aisenberg and Kimock about a decade ago.[22] In this technique, a bias voltage extracts the ions and directs them to the substrate. The Kaufman ion source, where electrons from a thermionic cathode are used with an axial magnetic field to generate a plasma, has been one of the most widely used ion sources. This design results in high deposition rates in a source gas such as methane. Positively charged species can then be extracted from the source by a bias electrode and pulled to a substrate. Good review papers on the Kaufman ion source and its applications are cited in Ref. 23. The driving force behind the use of ion beams lies in the better control available with ion beams than with other plasma sources. For example, an ion beam can be produced with a narrow energy distribution and specified direction. Important parameters such as beam energy and ion current density can be controlled almost independently over a wide range of process conditions. This is in sharp contrast to most plasma techniques in which bombardment conditions are controlled by a variety of parameters including plasma power, gas pressure, gas composition, flow-rate, and system geometry.[22] In addition, the separation of the ion generating plasma volume from the substrate minimises interaction between high energy plasma electrons and the substrate. As a result, high energy particle impact events occur only as a result of impingement of well defined ion beams.

In order to take full advantage of the control offered by the ion beam deposition technique, it is important to maintain the ion beam energy, beam current, and chemical identity of the ion species while transporting the beam to the substrate or target. In this regard, it is most important to minimise the pressure in the region of beam transport.

As pointed out by Aisenberg and Kimock,[22] essentially it is the impact of ions with energies in the range of a few electronvolts to kiloelectronvolts on the surface of a growing film that leads to the production of metastable materials with unique properties. Primary ion impact energies used to generate metastable materials are normally in the range 30–1000 eV.

There are two types of ion beam deposition. The first is direct ion beam deposition, where an ion beam of controlled composition, energy, and flux is directed onto a substrate. Figure 2 is a schematic illustration of the working principles of direct ion beam deposition.[22] The impacting ions in this technique are used to supply both the deposition atoms and the energy required for improved film formation. The very smooth nature of the deposited films is usually explained on the basis of surface energy considerations. The total surface energy is equal to the product of the surface tension and the surface area, and the drive to minimise total energy corresponds to a drive to a minimum area. The driving force is proportional to the surface tension and in the case of non-equilibrium atoms the surface tension is unusually large and thus produces a strong drive to a minimum surface area.

The second type of ion beam deposition is the so called ion assisted deposition.[22] Figure 3 is a schematic illustration of such a system. In this technique, one can produce films at a much faster rate and over a larger area than with direct ion beam deposition,

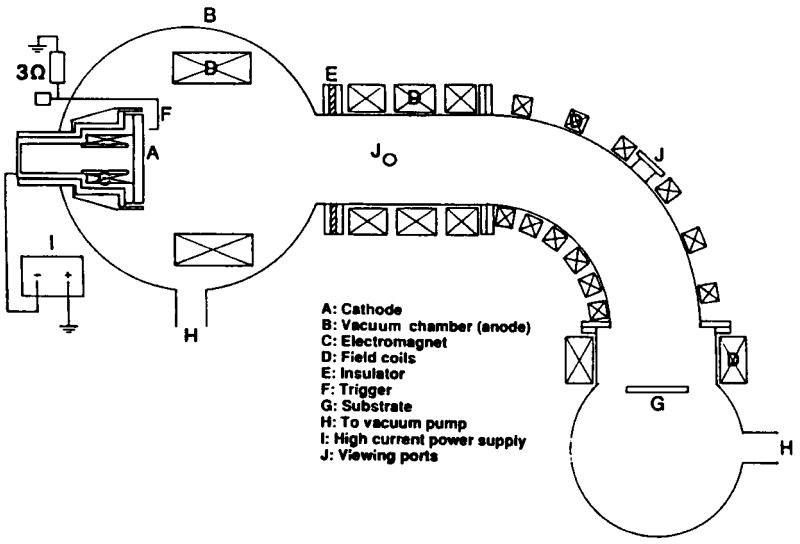

4 Schematic illustration of mass selected ion beam (MSIB) deposition system[10]

because there is no need to produce ions of the material to be deposited. In this case, the non-equilibrium ion energy is provided by a gaseous ion source operated in parallel with the source of atoms or clusters of the material to be deposited.[24] This configuration still allows the deposition chamber to be maintained at a high vacuum, permitting retention of ion energy and minimising substrate contamination.

Apart from single ion source deposition, a dual ion source technique has also been used to deposit DLC films. The other source may be a dopant source, or just a means of producing energetic argon ions that bombard the growing films so as to promote sp^3 bonding.[25]

One modification of the ion beam deposition technique is the mass selected ion beam (MSIB) technique. A detailed review of the effect of various parameters on MSIB DLC film growth was given by Lifshitz *et al.*[26] These authors also proposed a growth model for DLC films, which is analogous to a subplantation model (subsurface shallow implantation). An MSIB system is illustrated schematically in Fig. 4. As can be seen, such a system can be much more sophisticated than standard ion beam systems. This technique makes it possible to deposit a single ion species by passing the whole ion beam through a magnetic mass analyser for electron/mass selection. The analyser is designed to filter neutrals, cluster species, graphitic fragments, and other undesired species such as impurities from the beam and to allow only a pure beam of C^+ (or C^-) ions to reach the substrate. The MSIB was first used by Aksenov *et al.*[10] and has now been used by several groups around the world.[21,27] Characterisation of DLC films produced by MSIB technique using electron energy loss spectroscopy (EELS) has indicated that these films have high fractions of sp^3 bonding.[21] Typical film growth rates are of the order of 40 nm min^{-1}.

A most recent study on carbon transport in Si (001) and nucleation of DLC layers during MSIB deposition showed that the substrate contains a large amount of carbon, according to secondary ion mass spectroscopy (SIMS) up to 1 at.-%, and the carbon content is found far beyond the depth of a few nanometres that would be expected from thermal diffusion and ion implantation. Discussions on the nucleation and growth of the DLC layer as a function of the deposition energy have correlated the mechanism to the subplantation model. The unusually deep penetration of carbon into the substrate can be interpreted in terms of a crowdion diffusion and mass transport mechanism that can be enhanced by silicon point defects created in excessively high densities as a result of carbon ion impact.[28]

The main drawbacks of MSIB reside in its very slow film deposition rate due to the limited beam size, and very high cost compared with CVD or plasma deposition. Therefore, throughput becomes a major concern for commercial applications.

Cathodic arc deposition

The ion flux emitted from a cathodic arc is closely related to the composition of the target and is highly energetic and excited. Thus, cathodic arc evaporation of a graphite cathode has been reported as a suitable process for the production of hard wear resistant carbon films over a large area.[29] Using this technique, both pure DLC films and doped DLC films can be processed with ease.[30,31] Figure 5 is a schematic view of the carbon deposition setup.[29] It includes an evaporator assembly, a vacuum chamber, the magnetic system of the cathode spot control unit, a consumable cathode, and a substrate holder with bias supply. The cathodic arc is a low voltage high current discharge in which the current flows from the cathode at one or more small cathode spots, 5–10 μm in diameter. The extremely high current densities at the cathode spot cause violent emission of the solid cathode material, most of which is then ionised in the intense plasma associated with the cathode spot. For a carbon cathode, the emitted material is primarily C^+ ions with kinetic energies characterised by a broad peak at abount 22 eV.[32] Sufficient plasma is emitted to make the discharge self-sustaining in a vacuum, and

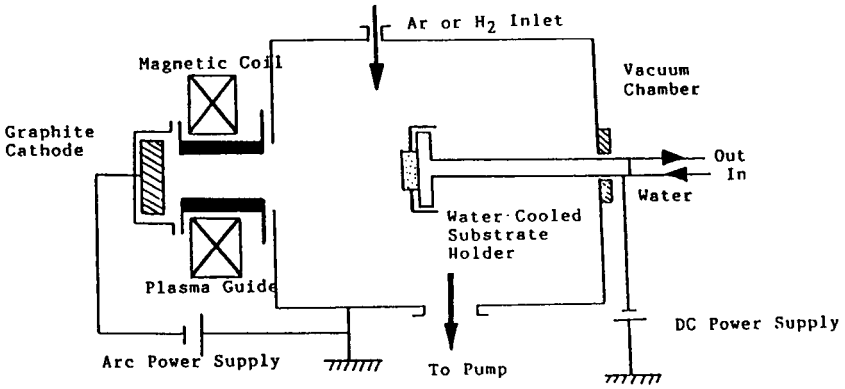

5 Schematic illustration of cathodic arc deposition system[29]

the cathodic arc is therefore often referred to as a vacuum arc.[33] A recent comprehensive review on cathodic arc deposition (CAD) of thin films (including DLC) has been given by Brown.[19]

The major modification of the conventional cathodic arc evaporation technique is the filtered cathodic vacuum arc (FCVA) deposition technique. The pioneering work in FCVA was due to Aksenov *et al.*[34] Figure 6 shows a schematic configuration of the experimental setup used by Aksenov. It consists of an arc plasma source, plasma duct, insulators, magnetic coils, vacuum chamber, collector (substrate), etc. During FCVA deposition, the neutrals and macroscopic particles are removed from the plasma streams, so that only the charged species in the plasma reach the exit and are deposited onto the substrate. Films of DLC prepared using a FCVA are found to possess high hardness and density.[35] The high compressive stress (9–10 GPa) found in the DLC films made by FCVA indicates that the film quality is high and the sp^3/sp^2 ratio usually scales with the internal compressive stress.[30,36,37]

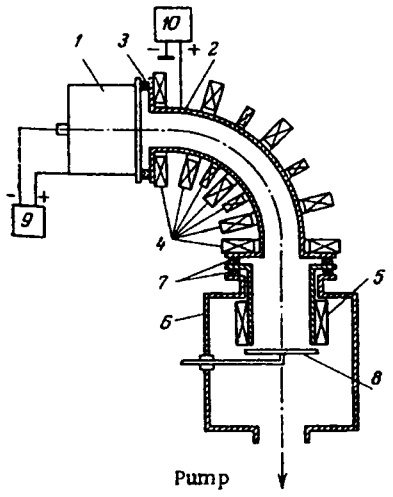

1 arc plasma source; 2 plasma duct; 3 insulator; 4, 5 magnet coils; 6 vacuum chamber; 7 insulator; 8 collector; 9 rectifier; 10 bias voltage supply for plasma duct

6 Schematic configuration of experimental setup for filtered cathodic vacuum arc (FCVA) deposition used by Aksenov[34]

Sputtering deposition

Various sputtering methods have been used to produce DLC films, either hydrogen free or hydrogenated, depending on the atmosphere and target material used. Ion beam sputtering techniques usually use an Ar^+ ion beam of typically 1 keV energy to sputter a graphite target.[38] The sputtered carbon species is then condensed on a nearby substrate. It has been demonstrated that a second Ar^+ ion beam to provide ion bombardment of the growing films might be essential to promote sp^3 bonding.[39] Researchers have also correlated the fraction of tetrahedral bonding to the energy of the incident bombarding Ar^+ ions,[40] and an optimum energy has been reported.[41] Also important is the relation between the energy of the incident bombarding Ar^+ ions and the internal compressive stress in the films. This is the basis for the subplantation mechanism proposed to explain the origin of the residual internal stress universally found in DLC films with high sp^3 fraction.[40]

The apparent disadvantage of ion beam sputtering is the low deposition rates that arise from the low sputtering rate of graphite. This can be overcome by using magnetron sputtering, which uses an Ar^+ plasma to sputter the graphite target and simultaneously bombard the growing film.[42,43]

Cuomo *et al.*[38] reported sputter deposition of dense DLC films at low temperatures and found that film density and sp^3 bonding character increase with increased substrate thermal conductivity and decreasing substrate temperature. They proposed a model for the condensation of energetic carbon atoms into diamondlike films in which a quench type surface accommodation mechanism is operative. However, this mechanism is untenable in details.

Magnetron sputtering has been the major technique used to produce DLC coatings in industry, because it offers good process control and can readily be scaled up to meet manufacturing requirements, including conformal coverage of the substrate. The disadvantage resides in the fact that the hardest films are formed under conditions of lower power and low gas pressure, where deposition rates can be reduced.

Laser ablation deposition

Laser ablation, or more specifically, pulsed laser ablation (PLA) and deposition of thin films has

gained tremendous popularity since the deposition of high T_c $Y_1Ba_2Cu_3O_{7-\delta}$ films in 1987 by this technique.[44] When the intense beam of photons impinges on a solid, the photons transfer their energy to electrons within 10^{-12} s (photon–electron interaction time $\sim 10^{-12}$ s), and the energy from the electron system is transferred to phonons within 10^{-10} s (electron–phonon interaction time $< 10^{-10}$ s). Thus, the photon energy ultimately appears as heat which can be used to produce melting and evaporation in a controlled way. In the melting regime, a simple heat balance can be used to estimate the depth of melting as

$$\Delta X_m = I(1-R)\tau/(C_V T_m + L)\rho \quad . \quad . \quad . \quad . \quad . \quad (4)$$

In the evaporation regime, the thickness of the evaporated/ablated layer is given by

$$\Delta X_m = I(1-R)\tau/(C_V T_m + L + \Delta H_V)\rho \quad . \quad . \quad . \quad (5)$$

In equations (4) and (5), I is the laser intensity (W cm^{-2}), C_V the specific heat, L the latent heat of melting, ΔH_V the evaporation enthalpy, ρ mass density, R reflectivity, and τ the pulse duration.

The average energy imparted to the laser ablated species is much higher ($(100–1000)kT$, where k is the Boltzmann constant and T absolute temperature). This characteristic feature makes possible stoichiometric evaporation, low temperature processing, and formation of novel phases.[45] The most interesting example of metastable phase formation at low temperature is carbon ablation, where pulsed laser ablation of sp^2 bonded carbon results in the formation of sp^3 bonded DLC. Narayan's group pioneered pulsed laser ablation of carbon to produce hydrogen free DLC films.[8] Singh and Narayan proposed a detailed model to account for the physical phenomena involved in the interaction of high powered nanosecond excimer laser pulses with bulk targets, resulting in evaporation, plasma formation, and subsequent deposition of thin films.[46] The removal of the material from the target by laser irradiation depends on the coupling of the beam with the solid. The thermal history (heating rate, melting, evaporation) during pulsed laser irradiation depends on the laser parameters (pulsed energy density E, pulse duration τ, beam shape, and wavelength λ), and the temperature dependent optical (reflectivity, absorption coefficient) and thermophysical (heat capacity, density, thermal conductivity, etc.) properties of the material.

Pulsed laser ablation of graphite targets has been used to prepare hydrogen free DLC films since 1989,[8,47] when this technique began to draw interest from the scientific and technological communities. Figure 7 is a schematic illustration of a typical pulsed laser deposition (PLD) system, the major components of which include a laser source, a high vacuum chamber, and pumping systems.

The special feature of PLA is that it is a non-equilibrium process and the species produced in the laser plasma possess very high kinetic energy. For instance, the average kinetic energy of atomic species produced by equilibrium processes such as electron beam evaporation is $\sim kT$, whereas that produced by pulsed laser ablation might be as high[48] as $(100–1000)kT$. The photon energy is such that it might enable a 2s electron to be promoted to the 2p orbital and so lead to the formation of the sp^3 hybridisation that is the precursor of DLC constituents. At present, PLD competes with FCVA and MSIB deposition techniques for the deposition of high quality DLC films. The decreasing cost of powerful excimer lasers and success in the development of PLD technology for large area deposition[44] (the current limit is areas 100–150 mm in diameter),[49] is expected to provide the basis for the introduction of PLD into general engineering fields.

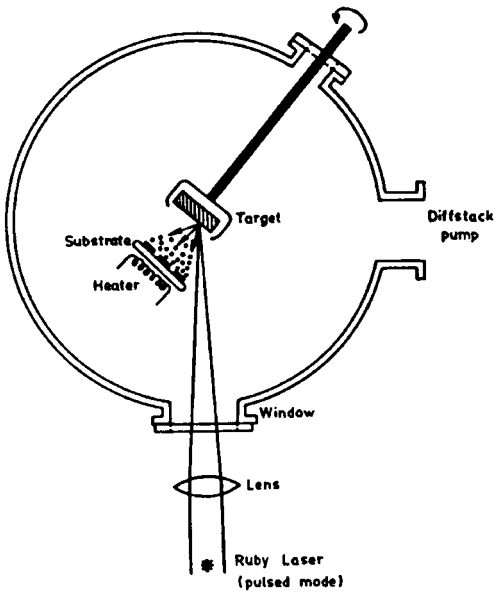

7 Schematic illustration of typical pulsed laser deposition (PLD) system: major components include laser source and high vacuum deposition chamber

Lasers with various wavelengths have been used to produce DLC films. The majority of early investigations used Nd:YAG lasers operating at 1064 nm.[50] Energy densities in excess of 100 J cm^{-2} have been used to deposit DLC films with 248 nm KrF excimer laser.[51] Film qualities such as transparency, sp^3 fraction, density, and internal stress are directly correlated with the energy density of deposition. The reported growth rates of DLC films deposited using 248 nm excimer lasers is of the order of 0·01 nm/pulse.[52] Experimental evidence suggests that superior DLC films with higher sp^3 fraction are produced at lower laser wavelengths. At a constant laser fluence of $\sim 3{\cdot}0$ J cm^{-2}, the excimer laser produced films are considerably superior to those produced with Nd:YAG (1064 nm) lasers. However, the difference between KrF (248 nm) and ArF (193 nm) produced DLC films is small, 68% for KrF versus 72% for ArF. These observations are consistent with detailed plasma plume diagnostic studies which clearly indicate the importance of C^+ species in enhancing the sp^3 fraction. These studies play down the role of diatomic carbon (C_2) species which tend to reduce the sp^3 fraction and degrade film quality. The plasma diagnostic studies support the hypothesis that the kinetic energy and momentum of vapour phase carbon species are key factors in the generation of sp^3 bonded states. These studies suggest that a kinetic

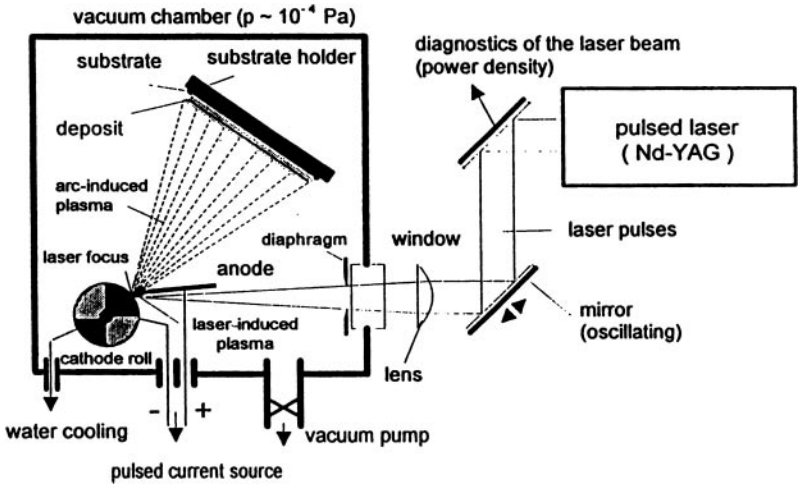

8 Schematic illustration of experimental arrangement for laser arc deposition technique[55]

energy of about 90 eV is optimal to produce a maximum fraction of sp^3 bonded carbon.[53]

The sp^3 content can be controlled within a wide range by monitoring the preparation parameters such as substrate temperature and material, as well as pressure and atmosphere in the deposition chamber. It has been corroborated that substrate temperature and atmosphere are the critical parameters, given the appropriate laser source and optical system, to achieve high quality DLC films with high sp^3 content. It has been shown that increasing the pressure of Ar and N_2 in the deposition chamber can enhance the formation of trigonal carbon (sp^2) content.[53] The likely explanation for this observation is that the kinetic energy of the carbon species in the plume is reduced with increasing pressure as a result of the increased probability of collisions (thermalisation).

A modification to PLD is the laser induced vacuum arc or laser arc (LA) technique. This makes use of a controlled pulsed arc plasma source combining the advantages of PLD with the high energy efficiency of a vacuum arc.[54] The basis of the LA technique has been described in detail by Siemroth and Scheibe.[55] Figure 8 is a schematic diagram of the experimental arrangement for the LA technique.[55] Evaporation is carried out in a vacuum chamber at a pressure of about 10^{-4} Pa, provided by a cryogenic pump. The plasma is produced by pulsed vacuum arc erosion of the cathode (target) material, placed in the chamber. The process control is realised by the use of a commercial Q switch Nd:YAG laser with a power density exceeding 5×10^8 W cm^{-2}. The laser pulse is focused on the cathode surface and produces a small plasma cloud that ignites the vacuum arc after arriving at the anode. The laser pulse length of about 100 ns is 2–3 orders of magnitude smaller than that of the arc pulses, while the energy of the laser pulses (a few millijoules) is much lower than the energy of the arc discharge (about 4·0 J). The material erosion occurs in the arc spot and is mainly dominated by arc conditions, the peak current and duration of arc pulses. The specifically developed power supply allows arc current pulses of between 100 and 20 μs duration, a maximum current of 1000 A, and a pulse frequency of up to 1 kHz. With these parameters, at a standard target to substrate distance of 150 mm, average deposition rates >10 μm h^{-1} have been achieved. No substrate bias is required and the deposition can be performed at substrate temperatures below 100°C. The cathode is designed as a roll of a pure material; for preparation of multilayered film structures it is suitably composed of different materials. Suitable laser control ensures that the entire surface of the cathode roll is eroded in a systematic and homogeneous way. In this way, films of pure metals, superhard amorphous carbon, and multilayered metal/carbon films can be deposited.

Studies using plasma diagnostics show that the LAD process is characterised by a nearly fully ionised plasma. For example, using optical emission spectroscopy (OES) it has been found that laser arc plasma reveals the highest degree of ionisation (claimed to be 100% C^+ ions) at a peak arc current of 1 kA. The kinetic energy estimated by Doppler shift of the spectral lines is about 20 eV, which is very close to the optimum energy for high quality DLC deposition.[56]

Diamondlike carbon films having Young's modulus up to 400 GPa and gap energies up to 2·0 eV have been produced by LA deposition.[54] The most significant advantage of using laser arcs is throughput. The growth rate of LA deposited DLC films is much greater than that of films obtained by techniques such as FCVA, MSIB, or conventional PLD. In comparison with the continuous arc, which is hard to control, laser induced and laser controlled pulsed vacuum arc deposition represents a way of controlling the erosion process of the material and reducing microparticle emission.

Plasma enhanced chemical vapour deposition

Plasma deposition or plasma enhanced chemical vapour deposition (PECVD) was the most popular method of producing hydrogenated DLC. It involves the rf plasma deposition of a hydrocarbon source onto a negatively self-biased substrate.[57] Since this review is focused on hydrogen free DLC, the details of this technique will not be discussed here.

Theoretical modelling and experimental characterisation of DLC

Since DLC is essentially an amorphous alloy combining sp^3 and sp^2 carbon, and their relative proportion changes substantially with many factors, a theoretical model concerning the structure, chemistry, physical characteristics, etc. has to allow for this feature of the system. Most earlier and contemporary characterisations have been focused on chemical bonding and various other factors that determine the chemistry of DLC, because essentially all properties of DLC films are in the end determined by their chemistry. Explaining the unique features of DLC in terms of theoretical models of the atomic structure, electronic properties, and other behaviour has been a great challenge. Pertinent factors include the short range order or medium range order compared with diamond and graphite, electronic structure, internal stresses, failure mode during service, and electronic processes (optical transitions, field emission, electrical conduction, vibrational behaviour (Raman and infrared), doping mechanism, etc.), and how these depend on the sp^3/sp^2 ratio. No theoretical models have been established that can account for all these aspects of DLC.

In the following, an account of the theoretical models developed to describe the structure and properties of DLC will be given. The techniques that have been used to characterise DLC films will also be described, with the focus on the sp^3/sp^2 ratio determination.

Theoretical modelling of DLC

One of the earliest theoretical models was proposed by Beeman *et al.*[58] They constructed three structural models of amorphous carbon with differing percentages of sp^3 and sp^2 carbon atoms, along with a purely sp^3 amorphous germanium model that was scaled to diamond bond lengths. For structural studies, they analysed the radial distribution function (RDF) which can give the short range order of the system. The model of a fully sp^3 structure was generated by rescaling the 519 atom Polk model[59] of amorphous germanium. The local electronic density of states of graphite, diamond, and the four theoretical structures constructed by Beeman *et al.*[58] is shown in Fig. 9. Two notable features of their models should be highlighted. First, with the exception of the pure sp^2 model, all the models correspond to relatively isotropic randomly connected networks with no interior dangling bonds. Second, all models were computer relaxed by the method of Steinhardt *et al.*[60] to minimise the strain energy resulting from distortion in bond length and bond angle from their crystalline values. Bearing these two features in mind, their conclusion that the proportion of sp^3 atoms is not likely to exceed 10% is not surprising. A structure that is free of dangling bonds cannot represent the realistic structure of amorphous semiconductors such as DLC; thus, large compressive stresses in DLC are required to accommodate high sp^3 fractions,[30] which is consistent with experimental observations.

Another important part of the work by Beeman *et al.*[58] is their analysis of the vibrational properties.

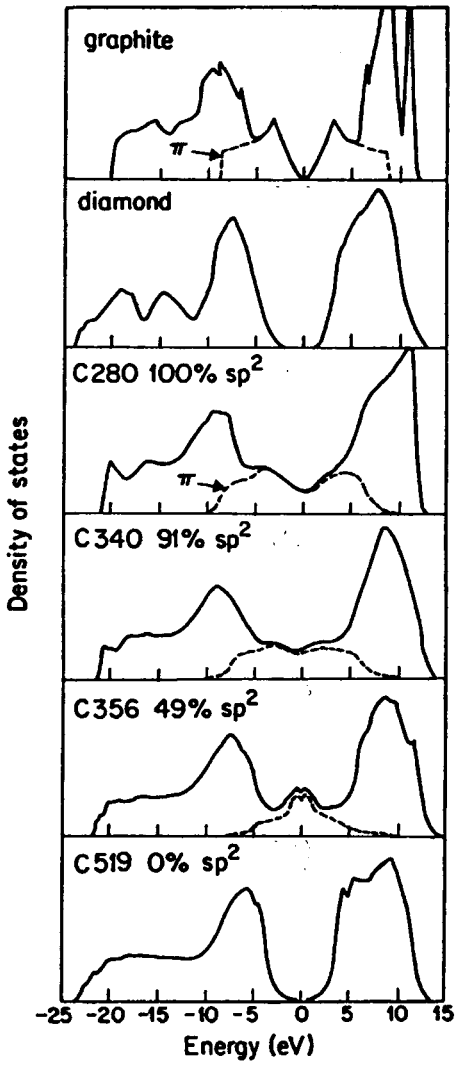

9 Local density of states plots for graphite, diamond, and four theoretical structures constructed by Beeman *et al.*:[58] from Robertson *et al.*[61]

They calculated the vibrational density of states (VDOS) and reduced Raman intensity for the models. The calculated VDOS for the models and the calculated reduced Raman spectra for the different structures are compared with the experimental results in Fig. 10. The remarkable feature, to which the authors did not pay much attention, is a VDOS peak located at about 1200 cm^{-1} in the spectra for structures that have large sp^3 content. This peak corresponds to the amorphous sp^3 constituent but had not been experimentally detected until recently.

Robertson *et al.*[61] calculated the electronic and atomic structures of amorphous carbon based on the Hückel approximation and described the electrons by a tight binding Hamiltonian, which uses an sp^3 basis set and retains only first neighbour interactions and some second neighbour interactions. The formation of the band gap, the possibility of doping, and atomic arrangements were studied. The existence of a gap in π states was analysed by neglecting the σ states entirely, because π states lie closer to Fermi level E_F and because, to first order, local symmetry decouples

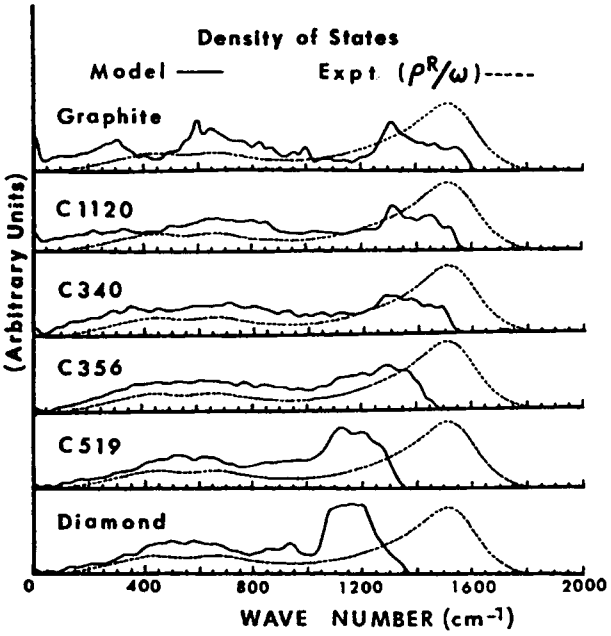

10 Calculated vibrational density of states plots of Beeman *et al.*[58] and reduced Raman intensity for four models of Beeman *et al.*

them from the σ states. As can be seen from the calculations of Beeman *et al.*,[58] a key feature of the π states is that they are half filled, so that creating a gap in their spectrum at E_F will tend to lower the total π electron energy per atom E_{tot}, and thereby stabilise the new structure. Thus, the driving force giving the gap in DLC is that this tends to lower π electron energy. This is opposed by the σ backbone whose energetics can be described by a valence force field of bond stretching and bond bending forces. Therefore, it is clear that the gap will depend primarily on the concentration and disposition of the π states, and only indirectly on other factors such as hydrogen content, although a different conclusion has been reached by other investigators.[62] Robertson *et al.*[61] found that the most stable arrangement of sp^2 sites is in compact clusters of fused sixfold rings, i.e. graphitic layers. The width of the optical gap is found to vary inversely with the sp^2 cluster size, and the $\sim$0·5 eV optical gap of evaporated amorphous carbon is found to be consistent with a model of disordered graphitic layers of about 15 Å diameter, bounded by sp^3 sites. It is argued that DLC forms such finite clusters in order to relieve strain. This then implies that the optical gap of DLC depends on the degree of medium range order, rather than just on the short range order as is the case in most amorphous semiconductors. The authors argued that the states in the gap (defect states) are expected to arise from atoms with an atypical coordination. Unlike other amorphous semiconductors that are all σ bonded, in a system such as amorphous carbon, containing both π and σ bonding, there is in principle the possibility of both π and σ defects. However, since π bonding is weaker, one would expect π defects to predominate due to their lower creation energy. It is demonstrated that any cluster with an odd number of π orbitals will produce a state near $E=0$ and that it will be half

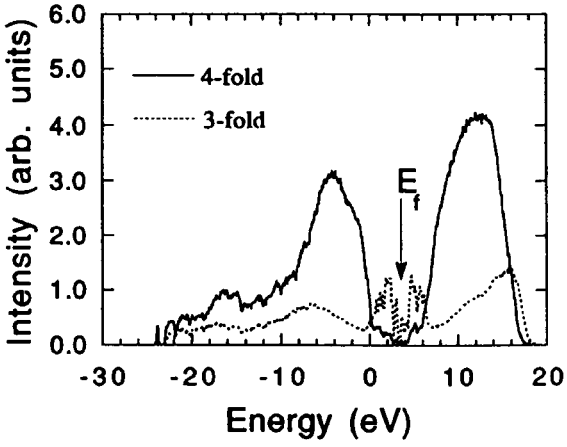

11 Electronic density of states plots for tight binding molecular dynamics generated DLC network of Wang and Ho[66]

filled. In the work of Robertson *et al.*,[61] only doping in a-C:H is discussed.

Tersoff performed calculations with an empirical potential, which suggest that an sp^3 bonded network would be severely strained; he therefore suggested that the equal sp^2 and sp^3 content could be more plausible.[63] It now seems clear that Tersoff's model structure is not representative of DLC since unambiguous experimental evidence of sp^3 contents approaching 90% has been obtained.[64]

Drabold *et al.*[65] reported theoretical studies of DLC using *ab initio* density functional methods. The primary result of their effort is the pairing of three-coordinated defects in the amorphous network. When this happens, a large optical gap of more than 2·0 eV appears, completely free of defects, in agreement with experiments. Calculations of the vibrational properties of their DLC network also give a spectrum similar to that of Beeman *et al.*,[58] i.e. peaks occurring at around 1200 cm^{-1}. They proposed that the vibrational, and especially the electronic, properties are much more sensitive measures of a model structure than, for example, RDF analysis.

Wang and Ho[66] generated an amorphous carbon network by quenching high density, high temperature liquid carbon using tight binding molecular dynamics simulations. They found that the network thus created contains a large fraction of sp^3 sites (74%). Studies of the structural, vibrational, and electronic properties of the theoretical model showed general agreement with available experimental results. The electronic DOS of DLC calculated by Wang and Ho[66] is shown in Fig. 11. The total electronic DOS is very similar to the broadened DOS of diamond except for the appearance of some states in the gap region. Decomposition of the electronic DOS into contributions from sp^3 and sp^2 atoms shows that the states in the gap region are mostly due to the threefold atoms which exhibit a pseudogap of about 2·0 eV, while the states associated with the fourfold atoms have a gap of about 5 eV. The vibrational DOS of DLC, diamond, and graphite are shown in Fig. 12. Again, their calculated VDOS showed peak density at around 1200 cm^{-1}, in agreement with Beeman *et al.*[58] and Drabold *et al.*[65]

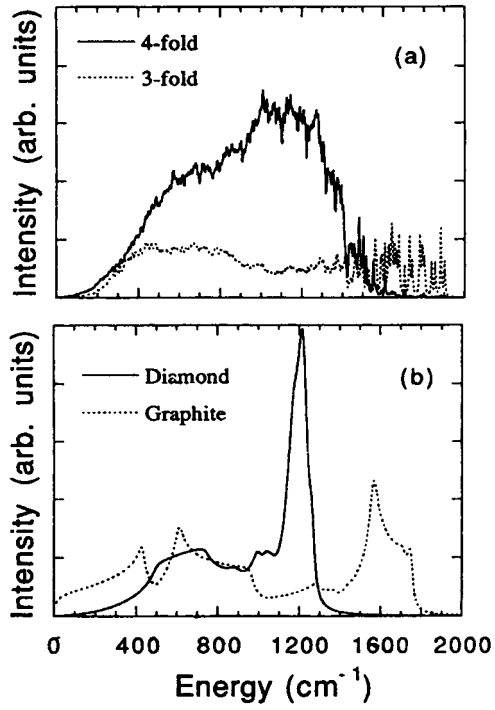

a threefold and fourfold atoms in DLC network; *b* in graphite and diamond[66]

12 Vibrational density of states plots[66]

Further discussions on the electronic structure and electronic doping will be given below with regard to the electronic and electrical properties of DLC.

Experimental characterisation of the structure and chemistry of DLC

The most widely used experimental characterisation techniques for the structure and chemistry of DLC include visible and ultraviolet Raman spectroscopy, FTIR spectroscopy (for hydrogenated DLC, in particular), TEM, and X-ray photoelectron spectroscopy (XPS).

Raman spectroscopy

Raman spectroscopy has been the most extensively used technique to study the bonding states of various phases of carbon. The characteristics of Raman spectra for diamond and graphite crystalline phases have been well established. In diamond, either natural or synthesised, a Raman peak around 1332 cm^{-1} has long been identified, although the specific peak position depends on the stress conditions in the diamond crystal.[2] In the case of single crystal graphite, a single peak located at 1575 cm^{-1} has been identified.[67]

The Raman scattering process involves inelastic light scattering from vibrational excitations in the sample.[68] For crystalline samples, the Raman spectra are due to vibrations with a wavelength determined by the scattering geometry and $\boldsymbol{k}$ vector conservation (or $\boldsymbol{k}$ selection rule). Because the wavelength of light is long on the scale of phonon wavelengths, these requirements select only wavevectors with $\boldsymbol{k} \sim 0$, or Brillouin zone centre excitations. Thus, Raman spectra of crystalline phases will display sharp peak(s) representing the zone centre mode(s).

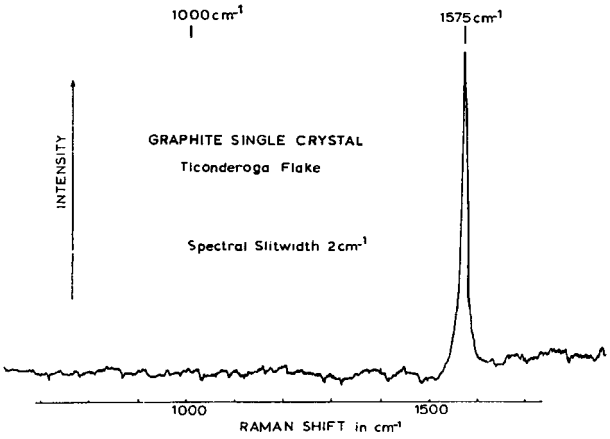

13 First order Raman spectrum of single crystal graphite obtained by Tuinstra and Koenig[67]

In amorphous materials, lattice absorption processes involving phonons are retained to a degree that depends on the material, but the fine features are lost. A relaxation of the $\boldsymbol{k}$ vector selection rules that govern the vibrational properties in the crystalline state allows coupling to modes that are not active in crystals, so that Raman and infrared activity extend over the entire vibrational spectrum, often giving broad humps rather than characteristic sharp peaks.[69]

Since the atomic structure and the bonding characteristics of most DLC materials are between those of diamond and those of graphite, in order to gain a full understanding of the vibrational properties of amorphous DLC it is helpful to start with a detailed description of the two extrema.

The initial first order Raman spectroscopic studies on graphite were by Tuinstra and Koenig.[67] Before their experimental work, several theoretical investigations on the lattice dynamics of graphite had been reported.[70,71] For single crystal graphite, a single peak was observed at 1575 cm^{-1}, and changing the orientation of the sample with respect to the incident radiation did not change the spectrum. Figure 13 shows the first order Raman spectrum of single crystal graphite obtained by Tuinstra and Koenig.[67] However, in the case of polycrystalline graphite, an additional line is observed near 1355 cm^{-1}. The relative intensities of the two lines depend on the type of graphitic material being examined. The intensity of the 1355 cm^{-1} peak increases as one goes from stress annealed pyrolitic graphite through commercial graphite to carbon black. This increase corresponds, first, with an increase in the amount of 'unorganised' carbon in the samples; and, second, with a decrease in the graphite grain size. The Raman spectra of stress annealed pyrolitic graphite, a commercial graphite, and activated charcoal are compared in Fig. 14. As demonstrated by later investigations, the Raman line at 1575 cm^{-1} is present in all the graphite samples studied. A slight frequency shift ($\sim$15 cm^{-1}) toward higher wavenumber was found in some samples with extremely small grain sizes. This band does not depend on the mutual arrangement of the graphite planes since it appears at the same frequency in those of graphite samples with only two-dimensional crystallinity.

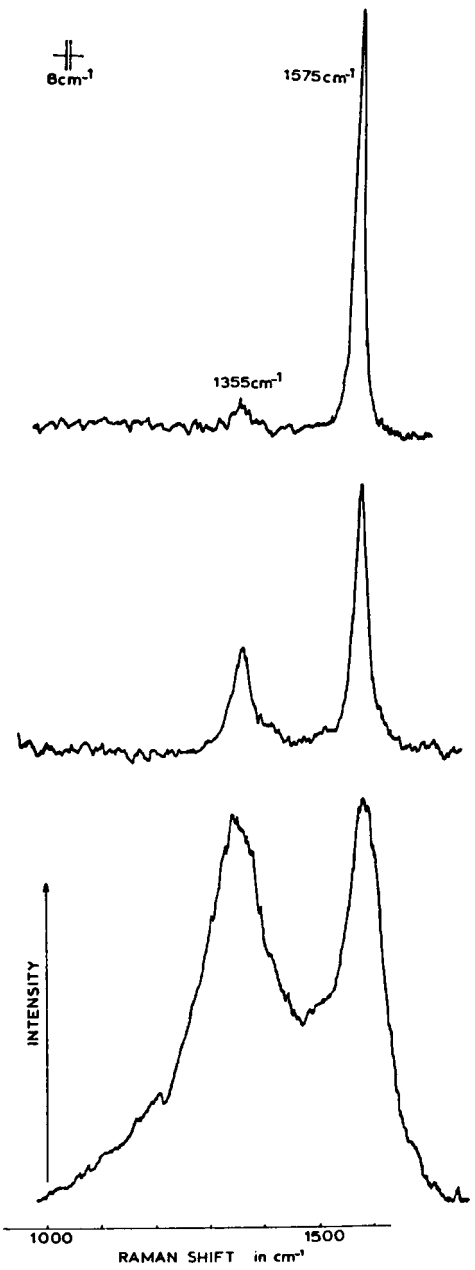

14 Raman spectra of stress annealed pyrolitic graphite (top), commercial graphite (centre), and activated charcoal (bottom)[67]

To understand the occurrence of Raman peaks of graphite, it is necessary to invoke the atomic structure and symmetry of a graphite crystal. There are four atoms in the unit cell of graphite so the phonon dispersion relation will reveal nine optical branches ($3N-3=9$, with $N=4$). Raman or infrared activity for a crystal can be observed only in the limit where the wave vector $\boldsymbol{k}=0$ ($\boldsymbol{k}$ selection rule). The unit cell has symmetry consistent with the space group D_{6h}^4. The point group homomorphic with this space group is D_{6h}. From the properties of this point group and the requirement that all unit cells must vibrate with the same phase ($\boldsymbol{k}=0$ or corresponding to the totally symmetric mode of the translation lattice), the symmetry properties of the normal modes can be calculated. The results are (the irreducible representation of the symmetry group)

$$2B_{2g}+2E_{2g}+A_{2u}+E_{1u}$$

Of the above modes, only the $2E_{2g}$ modes are expected to be Raman active as fundamentals. The symmetry of the E_{2g} modes restricts the motion of the atoms to the plane of the carbon atoms. The two different E_{2g} modes in the three-dimensional analysis occur because adjacent planes can vibrate in phase or with opposite phase. The energy difference between these two modes is very small since the interlayer forces are relatively weak. Therefore, in single crystal graphite, the two E_{2g} modes do not show a measurable frequency separation and will appear as a single band. The Raman band observed in single crystals of graphite can be assigned to these E_{2g} modes and has been called the G band or G peak.

However, it is relatively difficult to understand the origin of the 1355 cm^{-1} peak observed in polycrystalline graphite specimens. Because the peak position is close to that of diamond, one may assume that it is due to a diamondlike atomic arrangement in the graphite samples, when a comparison is made with the Raman spectrum of diamond. This possibility is excluded from the following reasons:

(i) the intensity changes of the 1355 cm^{-1} peak are not linearly related to the inverse of the unorganised carbon content
(ii) this peak has a narrow bandwidth, whereas the 'non-organised carbon', which is highly disordered, should give a broad peak
(iii) one would expect a frequency shift downward from 1332 cm^{-1} instead of the observed shift, both from the distortion of the bonds and from a heating effect due to the laser radiation
(iv) unorganised carbon would not account for the polarisation effects observed for the 1355 cm^{-1} peak.

An interesting observation is the effect of grain size on the occurrence of the 1355 cm^{-1} peak. If the Raman intensity of this peak is plotted against the crystallite size L_a, a linear relationship can be obtained, implying that the Raman intensity is proportional to the population of 'boundary' in the sample. Therefore, the 1355 cm^{-1} peak may be attributed to a change in the selection rules for Raman activity of certain phonons which were inactive in the infinite lattice. These kinds of 'end effects' on the Raman excitations have been reported for polymers. If the small crystallites can be considered to be big molecules with different sizes and shapes, then the only new Raman active modes are of the A_{1g} type. Figure 15 shows the first Brillouin zone of the two-dimensional graphite lattice.[67] All the points inside the zone or on the boundaries represent possible phonons. Owing to the irregular boundaries it is possible to reject standing waves resulting from reflection at the boundaries, leaving phonons corresponding to the point $\boldsymbol{k}=0$ and the boundaries of the first zone which represent internal standing waves. The point $\boldsymbol{k}=0$ has the full symmetry of the lattice (D_{6h}) and gives E_{2g} Raman mode vibrations. The only other point that has sufficient symmetry to give rise to an A_{1g} mode is the point $\boldsymbol{k}_1$, which is equivalent to points $\boldsymbol{k}_2$ and $\boldsymbol{k}_3$. These points in reciprocal space

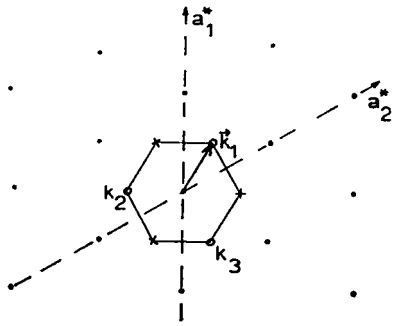

15 First Brillouin zone of two-dimensional graphite lattice[67]

have symmetry D_{3h}. The eigenvectors and eigenvalues can be calculated from a secular equation, and the eigenvectors show that there is an A_{1g} type mode at the $\boldsymbol{k}_1$ point. In an infinite crystal, this mode will be Raman inactive since the changes in polarisability cancel over the infinite crystal. For small crystallites, this is not so and Raman activity can be observed. Therefore, the 1355 cm^{-1} peak of graphite can be attributed to this A_{1g} mode of the small crystallites, or boundaries of large crystallites.

Because the appearance of the 1355 cm^{-1} peak is related to some extent of disorder in the graphite sample, it has been designated as the D peak or D band.

The Raman spectrum of diamond has long been established. For first order Raman scattering, only a single peak, located at 1332 cm^{-1}, has been identified. This line is from the zone centre optical phonon with $\Gamma^{(25+)}(F_{2g})$ symmetry. Diamond belongs to the space group O_h^7 with two atoms per primitive cell, and it is well known that it possesses one triply degenerate zone centre optical phonon with $\Gamma^{(25+)}(F_{2g})$ symmetry. This is the only mode which is Raman active in the first order.

Apart from loss of long range order in DLC compared with diamond and graphite, an additional fact adds to the complexity of Raman spectroscopy of DLC, especially its interpretation and relevance to the structure of the material. In amorphous silicon or germanium, the bonding state (sp^3) does not change significantly. Therefore, interpreting these Raman spectra is relatively easy compared with their crystalline counterparts. For example, the selection rule breakdown concept developed by Shuker and Gammon can be applied to understand the Raman scattering measurements of amorphous silicon and germanium.[72] They showed that in covalent semiconductors, where the bonds between atoms are similar to those in the crystalline phase, with nearly the same coordination number, bond length, and bond angles, the electronic structure of an amorphous semiconductor is only slightly disturbed relative to its crystalline counterpart.[59] In a simple approach, for example, the first order Raman scattering of amorphous covalent materials corresponds to the broadened VDOS. This simple model has been verified in the case of most tetrahedrally bonded amorphous semiconductors such as a-Si.[73]

In the case of DLC, however, the predominant difficulty in interpreting the Raman spectrum lies with the existence of both sp^2 and sp^3 bonding. For instance, there has been some controversy as to whether the visible excitation Raman features are from sp^2 or sp^3 species in the sample.[74,75]

The majority of the reported Raman studies of DLC have used visible wavelengths, mostly the 514·5 nm line of an argon ion laser.[68,74,75–79] It has been generally observed[68,76] that a relatively sharp Raman band occurs at $\sim$1560 cm^{-1}, and a broad shoulder band at $\sim$1350 cm^{-1}. Essentially, the major features of the visible Raman spectra of a-C films appear to be derived from corresponding features in the spectrum of graphite.[79] The so called G peak corresponds to the G line associated with the optically allowed E_{2g} zone centre mode of crystalline graphite and the D peak roughly corresponds to the D line associated with the disorder allowed zone edge mode of graphite. One of the basic controversies regarding the visible Raman spectra of DLC is on the origin of the two bands. For example, Wagner *et al.*[74] have divided Raman spectra of a-C films into two phases. They have assigned phase 1, at $\sim$1400 cm^{-1}, to vibrations originating from sp^3 clusters because of a resonant enhancement of phase 1 by excitation energy at 4·8 eV near the σ–σ^* transition energy of sp^3 bonded carbon. Yoshikawa *et al.*,[75] Nemanich *et al.*,[68] Tamor and Vassell,[79] and Tallant *et al.*[51] favour the graphitelike origin of the G and D bands. Yoshikawa *et al.*[75] have carried out EELS, optical absorption measurements and FTIR measurements, as well as Raman spectroscopy, in order to clarify this controversy and elucidate the origin of the Raman bands of DLC. They clearly showed that the shoulder band (D band) intensity increases with increasing substrate temperature: EELS shows two peaks due to plasma oscillation of π electrons and $(\pi+\sigma)$ valence electrons at about 6·7 and 25 eV respectively. The intensity of the peak due to π plasmons also increases with increase of the substrate temperature, showing the same trends as the D band in the Raman spectra. Optical absorption and FTIR measurements show the same tendency. Therefore, it is considered that the intensity of the shoulder band relative to that of the G band increases with increasing sp^2/sp^3 ratio, which confirms the hypothesis that the shoulder band originates from sp^2 carbon clusters. Bearing in mind the fact that the Raman scattering cross-section of diamond in the visible excitation range ($9{\cdot}1 \times 10^{-7}$ cm^{-1} sr^{-1}) is much lower than that of graphite (5×10^{-5} cm^{-1} sr^{-1}), it should be obvious that Raman scattering by sp^2 carbon is dominant in the spectra of a-C films for visible excitations because of the π–π^* resonance. In principle, visible Raman spectroscopy *per se* cannot give direct quantitative information about the sp^3/sp^2 ratio, nor can it even give direct evidence for the presence of sp^3 atoms in a specimen.

For the direct detection of sp^3 carbon atoms, other techniques must be used, or another wavelength of incident light has to be employed to excite the σ–σ^* transitions. However, it has been found that the shape of the visible Raman spectra of DLC can give indirect information on the film quality.[51] It was found that, in the case of excimer pulsed laser deposited DLC, the films become more transparent with increased

deposition energy, indicating a decrease in sp^2 carbon structures. The Raman band due to structures incorporating sp^2 carbon atoms shifts to higher frequency and becomes narrower and more symmetric with increasing deposition energy. Its integrated intensity decreases as the proportion of sp^2 carbon atoms decreases. Thus, increasing deposition energy appears not only to reduce the overall proportion of sp^2 carbon atoms, but also to narrow the distribution of structures in which they reside, resulting in a smaller spread of vibrational energies. While the band shift may be related to changes in the stress conditions in the films, other changes such as symmetry and integrated intensity of the G band still need further theoretical clarification. The vanishing of the D band from the Raman spectra of DLC with high sp^3 contents suggests the absence of any graphitic microcrystallites. Prawer *et al.*[80] have studied the systematic variation of the Raman spectra of DLC films as a function of sp^2/sp^3 ratio for hydrogen free DLC films. They indicated that the parameters from the fits show a strong dependence on the sp^2 component of the films. They further suggested that this might be used to identify unambiguously hydrogen free DLC films of low sp^2 content. However, the experimental results showed that the G peak position of the films is almost constant for sp^2 fraction below 40%.

Nemanich *et al.*[68] showed a strong spectral feature in the Raman spectra of DLC at $\sim 1140\,cm^{-1}$. They did not attempt to account for the appearance of this peak, but intuitively mentioned that this peak might come from some precursor of diamond. Four years before the work of Niemanich and co-workers, Beeman *et al.*[58] reported a theoretical model of a-C that gave reduced calculated Raman intensities. A peak close to $1200\,cm^{-1}$ was given for structures containing relatively large amount of sp^3 carbon.

It has been established that the $\sim 1200\,cm^{-1}$ peak comes from sp^3 carbon in the amorphous phase. Apart from a number of theoretical predictions,[58,65,66] Raman scattering from diamond that had been implanted with megaelectronvolt ions at beyond the critical ion dose required to turn the surface diamond into amorphous diamond, showed[81] a broad peak at $1200\,cm^{-1}$, which is in good agreement with the approximate one-phonon density of states for sp^3 amorphous carbon. Paillard *et al.*[82] produced DLC films through an approach called 'random compact cluster stacking'. They studied the vibrational properties of the DLC films using microscale Raman spectroscopy and compared the experimental results with theoretical predictions. Surprisingly, they observed three Raman bands, two of which were labelled D and G as usual. They considered the third band to originate from sp^3 components.

More recently, direct observations of sp^3 bonding in DLC films have been achieved in practice by the use of ultraviolet Raman spectroscopy.[51,83,84] Shorter wavelengths, such as violet light are used to enhance the resonance of the σ–σ^* electronic transitions. Ultraviolet Raman spectroscopy has been employed by chemists for several years.[85] In particular, it has emerged as a highly sensitive and selective technique for studying the vibrational spectra of molecules which have electronic transitions in the region

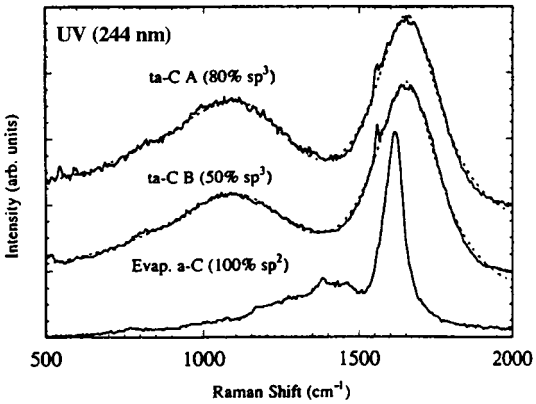

16 Ultraviolet Raman spectra for DLC and a-C containing various amounts of sp^3 carbon[84]

between 180 and 300 nm, driving the development of instrumentation capable of excitation in this region.[85] With this technique, a Raman peak at $\sim 1200\,cm^{-1}$ has been observed for largely sp^3 bonded DLC films. Examples of ultraviolet Raman spectra for highly tetrahedral carbon specimens, as well as evaporated amorphous carbon with 100% sp^2 carbon atoms, are shown in Fig. 16. It is clear that in addition to the G band, a peak located at $\sim 1100\,cm^{-1}$ is present in the highly tetrahedral carbon film. This peak is designated the T peak, which the authors attributed to sp^3 bonding for the following reasons:

(i) the size of this peak relative to the G peak decreases with decreasing sp^3 content, from film A to film B (Fig. 16), and scales approximately with the proportion of sp^3 sites in the two samples measured using EELS

(ii) the position of this peak is close to the main peak seen in the VDOS calculated by Beeman *et al.*,[58] for a fully sp^3 bonded continuous random network. It agrees well with calculations of VDOS by other groups of amorphous carbon that is not fully sp^3 bonded, but consists largely of sp^3 bonding

(iii) Nemanich *et al.*[68] and other researchers have observed similar results from CVD carbon films or ion implanted amorphous diamond (fully tetrahedral); EELS measurements have been used to calibrate the ultraviolet Raman studies. The experimental results are found to be in excellent agreement with theoretical predictions and have contributed to an improved understanding of the mechanism by which the diamondlike fraction develops within the amorphous carbon network.

It can be predicted that ultraviolet Raman spectroscopy will receive increased attention in the near future for DLC characterisation. While this may be so, Raman spectra obtained using visible excitation wavelengths show changes in the transparency of the film and the distribution of structures incorporating sp^2 carbon atoms. The carbon Raman band patterns from structures incorporating sp^2 carbon atoms correlate with the film density and internal stresses. Therefore, the distribution of structures incorporating sp^2 carbon atoms reflects, at least to some extent, the overall structure and properties of the carbon films,

and visible Raman spectroscopy is still a useful characterisation tool.[51]

Electron microscopy studies of DLC thin films

Transmission electron microscopy, especially with an EELS attachment, has been used to study the microstructure (atomic structure) and bonding states of DLC. Radial distribution function or reduced density function (RDF) analysis has been applied to the electron diffraction patterns to acquire atomic structure information on DLC. Some investigators have also employed X-ray diffraction and neutron diffraction to acquire atomic structure information of DLC thin films. In the following, work on atomic structure analysis and bonding characterisation is reviewed separately.

Structure analysis by diffraction and RDF Theoretical descriptions and applications of RDF analysis to DLC have been given by Cockayne and McKenzie,[86] who also give a brief derivation of the relevant equations.

A reduced intensity function is defined as

$$\phi(s) = \int_0^\infty [\rho^R(r, s) - \rho_0] 2r[\sin(2\pi sr)/s] \, dr \qquad (6)$$

where $\rho^R(r,s)$ is the atomic density as a function of r and s, ρ_0 is the average density, r radius, and s the scattering vector. Fourier inversion then yields the RDF

$$G(r) = 4\pi r[\rho^R(r) - \rho_0] = 8\pi \int_0^\infty \phi(s) \sin(2\pi sr) \, ds \qquad (7)$$

The function $G(r)$ describes the deviation of $\rho^R(r)$ from ρ_0, the total average atom density in the sample. From equation (7), a maximum in $\rho^R(r)$ (and hence in $G(r)$) will correspond to a maximum in an individual $\rho_{ij}(r)$, say $\rho_{kl}(r)$, if the $\rho_{ij}(r)$ do not overlap. Under these conditions, maxima in $G(r)$ give the most probable distances between atoms of types k and l. The identification of these distances with particular types of atom can often be inferred from knowledge of relevant crystalline structure.

Electrons have a number of advantages over other forms of radiation for the structural analysis of amorphous thin films. The most important is the large scattering cross-section which, combined with the availability of intense beams, permits rapid data collection with good statistics. Additionally the small wavelength compared with X-rays and neutrons allows collection of data to large values of scattering vectors $s = 2(\sin\theta)/\lambda$, and hence good spatial resolution. Electron diffraction has been utilised mainly to obtain short range structural information such as RDFs for amorphous phases. For DLC, since it has both fourfold and threefold coordinations, the first and second coordination spheres in the RDF should have coordination numbers between those of graphite (3, 6) and those of diamond (4, 12). Comparison of the RDF of DLC against those of graphite and diamond should shed light on the atomic structure of DLC.

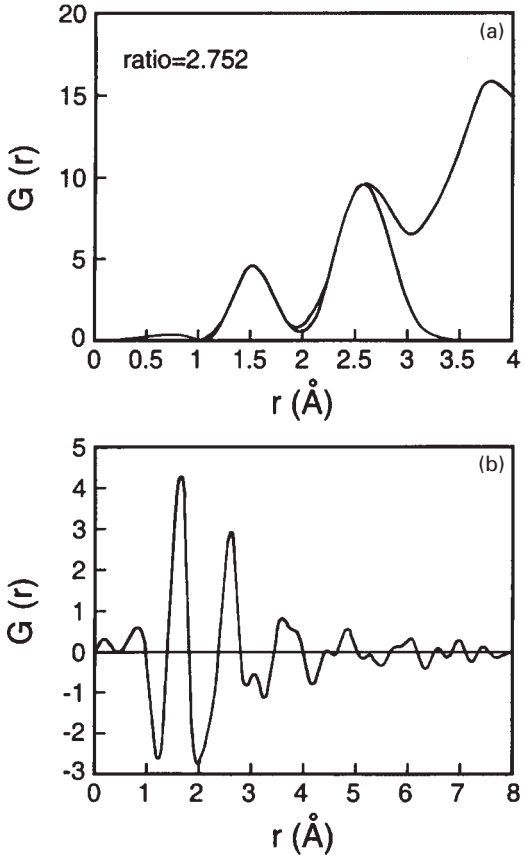

17 ***a*** **radial distribution function (RDF) obtained from electron diffraction of DLC prepared by pulsed laser deposition;** ***b*** **reduced RDF corresponding to** ***a***

To facilitate comparison, the number and distance of the first four coordination spheres of graphite and diamond are given in Table 1.

Figure 17*a* shows the RDF calculated from the electron diffraction data of a DLC sample prepared by PLD. The first and second nearest neighbour distances obtained from RDF analysis are 1·51 and 2·52 Å respectively. The ratio of the second shell coordination number to the first shell coordination number from RDF analysis is approximately 2·75. The reduced RDF corresponding to Fig. 17*a* is shown in Fig. 17*b*. Comparison with the data given in Table 1 for diamond and graphite suggests clearly that the DLC sample should possess a significant percentage of sp^3 bonded carbon atoms.

The results of RDF analysis, such as first nearest neighbour distance, second nearest neighbour distance, and the ratio of first to second shell coordination numbers, are given in Table 2, together with

Table 1 Number *n* and distance *r* of first four coordination spheres of diamond and graphite[87]

Coordination sphere	Diamond		Graphite	
	r, Å	*n*	*r*, Å	*n*
1	1·54	4	1·42	3
2	2·53	12	2·46	6
3	2·96	12	2·84	3
4	3·89	12	3·75	6

Table 2 Results of reduced density function (RDF) analysis for DLC and comparison with other forms of carbon: r_i and n_i are radius and number of coordination shell *i*

Carbon phase	r_1, Å	r_2, Å	n_2/n_1	Ref.
Graphite	1·42	2·45	2	87
a-C (sputtered)	1·46	2·49	2·1	88
Glassy carbon	1·425	2·45	2·1	87
a-C (evaporated)	1·43	2·53	2·6	89
Diamond	1·544	2·512	3	90
DLC film by PLD	1·51	2·52	2·75	91

data for diamond, graphite, and amorphous carbon made by other techniques such as sputtering. By comparing the first and second nearest neighbour distances and coordination numbers with those of diamond and graphite, it is clear from the data in Table 2 that the DLC film produced by PLD consists mainly of sp^3 carbon.

It is noted that most of the amorphous carbon materials studied in the past were predominantly sp^2 bonded.[87–89] Erroneous conclusions have been reached based on some models. To date, the number of diffraction studies on highly tetrahedral carbon ($\sim$80% sp^3 bonding) is quite limited.[56,64] One example is the work by Gaskell *et al.*[64] who used neutron diffraction on DLC films made by the filtered dc vacuum arc (FDVA) technique. Their DLC films had first nearest neighbour distances of 1·52 Å and a ratio of second to first shell coordination numbers of 2·8. Li and Lannin studied the RDF of thick amorphous carbon films prepared by rf sputtering in a high vacuum environment.[88] The macroscopic density of the a-C films was estimated from weighing selected samples to be only 2·0 g cm^{-3} and the film thickness was about 4 μm. Optical absorption and reflectance measurements yielded a Tauc gap of 0·57 eV. All these features merely imply that the a-C films were not characterised by a high content of fourfold coordination. The authors analysed the RDF obtained by neutron diffraction and obtained first and second nearest neighbour distances of 1·46 and 2·49 Å respectively.

Some RDF analyses based upon experimental diffraction results have also been compared with theoretical calculations. However, there is still considerable discrepancy associated with the theoretical modelling of the atomic structure of DLC and therefore care must be exercised when experimental RDF analyses are compared with the theoretical predictions.

A more comprehensive study on the atomic structure and physical properties of diamondlike carbon as simulated by a semiempirical molecular dynamics density functional approach has been performed by Frauenheim *et al.*[92] The authors reported detailed analysis of the reduced RDF on the basis of theoretical simulations and comparison with the experimental RDF obtained from electron diffraction of DLC specimens prepared by magnetron sputtering and arc evaporation techniques. Table 3 summarises some of their results. Sample a-C1 was prepared by magnetron sputtering, which yields low density material; samples a-C2 and a-C3 were prepared by FDVA deposition, which is known to produce high density DLC films. The experimental RDFs were obtained through electron diffraction analysis in a scattering vector range of $0{\cdot}5 \leqslant s \leqslant 23$ Å^{-1} using 100 kV electrons. The authors proposed that, for the reduced RDF, the following characteristics could be identified:

(i) the first correlation sphere is located at the mean bond length, indicating a shift to higher values for sp^3 enriched structures

(ii) the second correlation sphere results from an overlap of a distribution of next nearest neighbours and of higher order neighbours, and is therefore not a good candidate for deducing bond angle information

(iii) an interesting feature, a changing height ratio of the two correlation spheres, has been found, and can be correlated with an estimate of the sp^3 content and the network connectivity of the films. However, it appears that the theoretical modelling of Frauenheim *et al.*,[92] like those of most other investigators, tends to underestimate the sp^3 content. This tendency is clearly demonstrated by the data in Table 3.

Bonding characterisation by EELS Another important application of TEM to the studies of DLC films uses the EELS facility attached to some microscopes. It would appear that EELS has been the most widely used technique to obtain estimates of sp^3/sp^2 ratio.[21,93–96]

Generally, two parts of the EELS spectra are of critical importance for the characterisation of DLC: the low energy loss spectra; and the near *K* edge ionisation loss spectra. To extract information about the bonding of a DLC sample, it is common practice to use graphite, diamond, and other graphitised carbon samples as reference materials.[21,38,97] Figure 18 shows low loss spectra from several different forms of carbon: evaporated carbon (e-C), graphite, DLC, and diamond. The prominent peaks in these samples that are located at 25 eV for e-C to about 33·8 eV for diamond are due to plasmon excitations. It is found that graphite exhibits a resonance at a higher energy than does e-C, despite the similarity in chemical bonding in these two forms of carbon (both are all sp^2 bonded). This resonance shift has been attributed to a difference in density. However, it should be noted that graphite is highly anisotropic

Table 3 Comparison of structure data for real thin DLC films (Expl) with results of theoretical modelling by Frauenheim *et al.*[92] (Th)

	ρ, g cm^{-3}		sp^3, %		r_1, Å		r_2, Å		n_1	
Sample	Expl	Th	Expl	Th	Expl	Th	Expl	Th	Expl	Th
a-C1	2·0	2·0	10	15	1·46	1·45	2·5	2·55	3·0	2·78
a-C2	3·0	3·0	>80	53	1·51	1·51	2·53	2·49	3·8	3·53
a-C3	3·0	3·3	>90	83	1·55	1·54	2·57	2·53	3·8	3·81

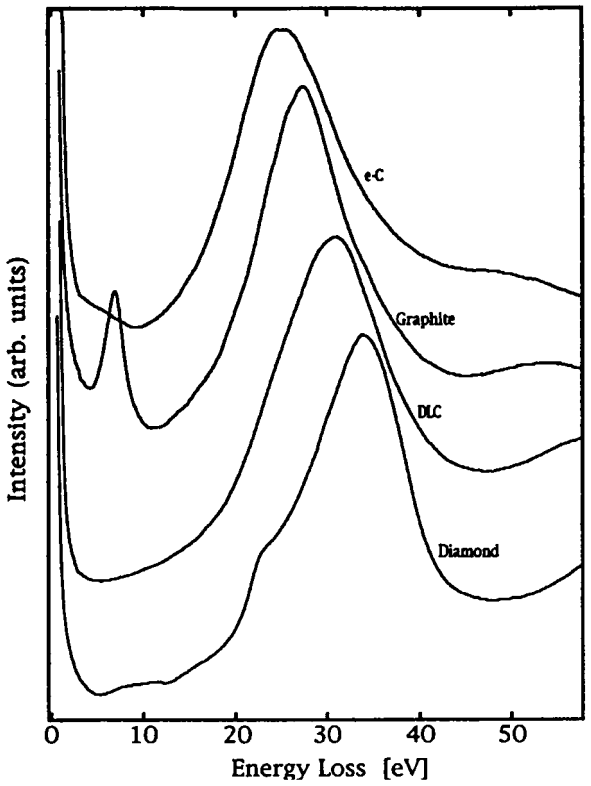

18 Comparison of low loss spectra from graphite, diamond, DLC, and evaporated carbon (e-C)[21]

and that the observed resonance energy depends on the orientation of the incident electron beam with respect to the axis of the sample. Therefore, care must be exercised when drawing quantitative conclusions regarding the density of the DLC films on the basis of comparisons of plasmon energies among different carbon allotropes. The graphite spectrum exhibits an additional feature at 7 eV, which has been referred to as either the π plasmon[98] or the π to π^* transition.[99] This feature has a counterpart in the e-C spectrum in the form of a broad, flat feature between 3 and 9 eV; however, it has no counterpart in the DLC spectrum, which exhibits no structure other than the broad plasmon excitation at about 30 eV. Diamond, on the other hand, shows at least three other features in addition to its bulk plasmon peak.[100] These are the band gap, which is visible as a rise in the loss signal beginning at about 6 eV in Fig. 18, with the specific value depending on the collection geometry;[21] the slope change at about 13 eV due to a strong interband transition; and the prominent shoulder at 23 eV. The origin of the last shoulder at 23 eV has been ascribed to surface plasmon excitation, an interband transition, or a contamination layer. In the low loss spectrum of DLC, the broad feature between 13 and 18 eV is analogous to the slope change at 13 eV in the diamond spectrum. Another broad feature which is somehow suppressed by the tail of the zero loss peak begin at about 5 eV, which might be correlated with the band gap in diamond at about 6 eV, although it could also be indicative of the π to π^* transition which might occur if the material is not purely sp^3 bonded.

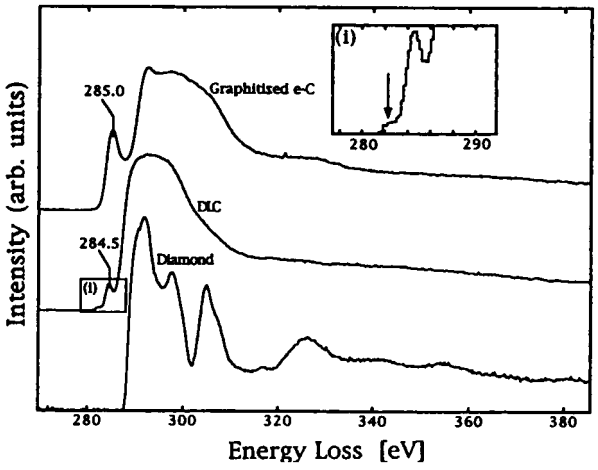

19 Comparison of *K* edge spectra from graphitised evaporated carbon (e-C), DLC, and diamond[21]

Another feature of interest in the low loss spectrum of DLC is the weak shoulder at about 24 eV. Its origin may be analogous to that in the spectra for diamond which exhibit a similar shoulder.

Adopting the simplest model for an insulating solid, then the peak in the EELS spectrum is expected to appear near the shifted resonance frequency,[98] giving

$$\tilde{\omega}_p = (\omega_p^2 + \omega_n^2)^{1/2} \quad \ldots\ldots\ldots\ldots (8)$$

Here ω_p is the plasmon frequency in the absence of binding and is proportional to the square root of the density, and ω_n is a phenomenological binding energy (e.g. a band gap). Some discrepancy from this analysis could be simply due to the erroneous assumptions of this model, i.e. that density is directly proportional to the square of the plasmon energy and that the constant of proportionality is the same for diamond and various forms of amorphous carbon.

By a comparative study of the low loss spectra of different allotropes of carbon, qualitative information can be obtained regarding the quality of DLC films. However, quantitative information such as the sp^3/sp^2 ratio of the specimens is usually obtained by analysing the *K* edge ionisation spectra. The *K* edge spectra from graphitised e-C, DLC, and diamond are compared in Fig. 19. Graphite single crystals are avoided as a reference because of graphite's anisotropy: the shape of its *K* edge spectrum is sensitive to the orientation of the incident beam with respect to the ***c*** axis of the sample. For use as a reference, the e-C sample must be fully annealed to ensure 100% sp^2 bonding with a random atomic network. It can clearly be seen that the π^* feature at about 285 eV is significantly reduced in the DLC sample compared with the e-C sample. The positions of the π^* maxima are indicated in Fig. 19. The value of 285·0 eV for e-C is lower than that for graphite, for which[38] the π^* feature peaks at 285·4 eV. The inset in Fig. 19 shows the detail of the edge onset in the DLC film. All films produce spectra exhibiting the weak shoulder indicated by the arrow in the inset. Although the origin of this shoulder is still uncertain, states within a presumed energy gap may give rise to this feature, since in an amorphous solid the matrix element for such transitions could be finite. The reduced π^*

feature in the DLC films is usually taken as an indication of a much lower fraction of sp^2 bonded atoms in DLC. Two methods have been proposed to calculate the sp^3/sp^2 ratio based on the K edge loss spectra of DLC. In the first method, proposed by Berger *et al.*,[97] the intensity of the π^* feature is taken to be directly proportional to the number of π bonded electrons in the material. The method is based on the 1s to π^* peak in the carbon K edge, because this feature is well defined in the spectra and the contribution to the leading edge of the peak from σ^* states is small in all forms of carbon. A measure of this intensity I_π is divided by the number of counts I_{Δ_E} within some relatively large energy window; ΔE is measured from the edge onset. If I_π is taken to be the number of counts from the edge onset to the minimum between the π^* and σ^* features, the ratio can be obtained by the following equation:

$$f^1 = I_\pi I^r_{\Delta_E} / I_{\Delta_E} I^r_\pi \quad \ldots\ldots\ldots\ldots (9)$$

where I^r_π and $I^r_{\Delta_E}$ are the appropriate integrals for the reference material, and f^1 refers to fraction of sp^2 bonded atoms in the specimen. This ratio has been normalised by the same ratio obtained for a reference material assumed to be 100% sp^2 bonded. The basic assumption of this method is that the matrix element for the transition from 1s to π^* states is invariant for all forms of carbon; further, that core hole relaxation effects are also invariant.

The second method was proposed by Cuomo *et al.*[38] In their work, spectra in the energy loss range from 280 to 310 eV were acquired. The peak in the region from 285 to 290 eV results from excitations of electrons in the ground state 1s core levels to the vacant π^* like antibonding states. Excitations to the higher lying σ^* states occur above 290 eV. To a good approximation, the ratio of the integrated areas under these two energy windows is proportional to the relative number of π and σ^* orbitals, which is 1 : 3 for 100% sp^2 and 0 : 4 for completely sp^3 bonded carbon. The atomic fraction of sp^2 bonded carbon x is determined for the range of samples using the expression

$$(I_\pi/I_\sigma)_s/(I_\pi/I_\sigma)_r = 3x/(4-x) \quad \ldots\ldots (10)$$

where I_σ is the integrated intensity in the range from 290 to 305 eV, I_π the intensity in the range from 284 to 289 eV, and the subscripts s and r refer respectively to the ratio determined for the DLC specimen and a reference material with 100% sp^2 bonding. It has been found that the second method yields lower sp^3 fractions than the first method.[21]

The uncertainty in EELS lies in the calibration procedure, which can lead to errors in experimental results. Another disadvantage of EELS is that it is a destructive test, and the film properties may be affected during TEM sample preparation or by high energy electron beam irradiation. The interband scattering between sp^3 and sp^2 states also contributes to the uncertainty in EELS analysis.

FTIR characterisation and infrared range optical properties of DLC films

The FTIR spectroscopy technique has been used predominantly for infrared studies of hydrogenated DLC (a-C:H) since C–H bond stretching or bending is infrared transition active. In most cases, FTIR has been used to confirm whether a DLC film is hydrogenated or not and what types of C–H bonding are present. Another important application of FTIR is to investigate the thermal stability of hydrogenated DLC films, particularly the behaviour of hydrogen atoms associated with thermal annealing.[101]

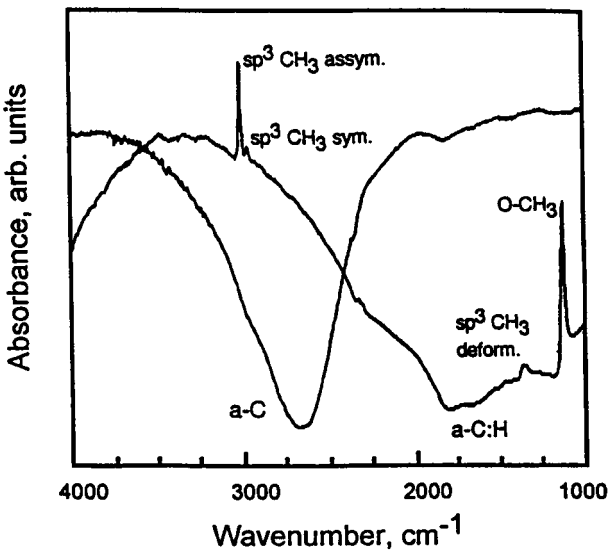

20 Fourier transform infrared spectroscopy absorption spectra for a-C and a-C:H films recorded in reflective mode from films deposited on steel substrates[47]

These FTIR measurements are important also because DLC films have been considered to be a promising candidate for infrared antireflective coatings. Knowledge of the infrared optical properties of DLC is crucial for this potential application and it is in this context that the ability to obtain FTIR measurements for hydrogen free DLC is imperative.

The infrared range transimittance, reflectance, emittance, absorbance, refractive index, and extinction constant, as a function of wavelength, are important properties. For hydrogen free DLC films, these properties are functions of chemistry and structure, especially the sp^3/sp^2 ratio, the surface roughness, and dopant concentration and dopant type.

Voevodin and co-workers showed that there is in general difference between the FTIR absorption spectra for a-C and a-C:H films in terms of spectrum shape and other characteristic features.[47] In the former, the peaks characteristic of CH_2, CH_3 or O–CH stretching or bending modes are absent. The FTIR absorption spectra of a-C and a-C:H films, recorded in a reflective mode from films deposited on steel substrates,[47] are shown in Fig. 20. The a-C film was deposited by PLD.

Another aspect of the infrared range optical characterisation of DLC is associated with the spectral emissivity behaviour. This can in principle yield information regarding the electronic DOS distribution, at least qualitatively.

A detailed description of the theoretical background of spectral emissivity of a semiconductor was given by Sato.[102] Briefly, emissivity is defined as the ratio of the radiance of a given object to that of a blackbody at the same temperature and for the same

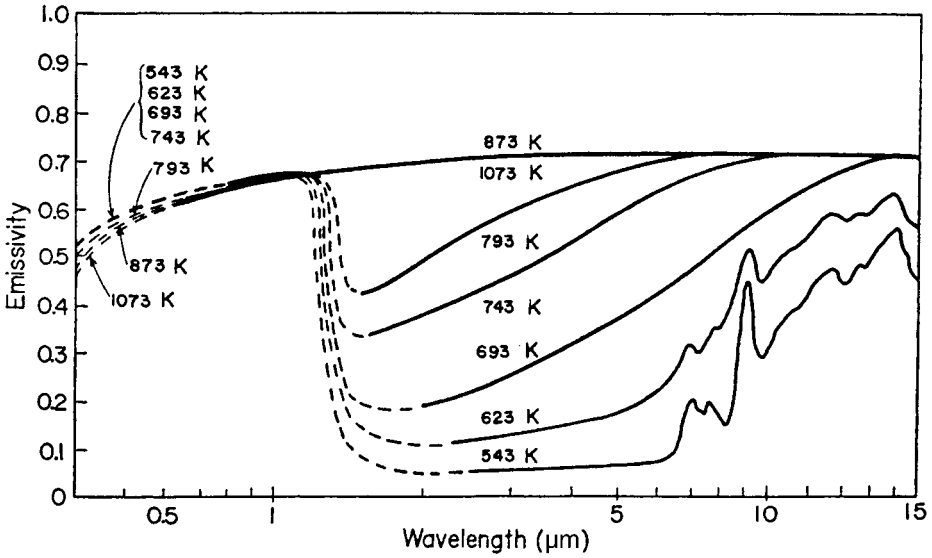

21 Emissivity spectra of intrinsic silicon at various temperatures[102]

spectral and directional conditions. It is a function of wavelength and temperature. For normal incidence, the emissivity ε of a plane parallel specimen can be written as

$$\varepsilon = (1-R)(1-T_r)/(1-RT_r) \quad \ldots\ldots\ldots \quad (11)$$

where R is the true reflectivity and T_r is the true transmissivity. For a perfect opaque body, for example when the absorption coefficient α and the film thickness t are such that αt is large and $T_r \approx 0$, we have Kirchhoff's law

$$\varepsilon = 1 - R = 4n/[(n+1)^2 + k^2] \quad \ldots\ldots\ldots \quad (12)$$

If the apparent reflectivity and transmissivity that are actually measured experimentally are denoted by R^* and T_r^*, the relation

$$\varepsilon + R^* + T_r^* = 1 \quad \ldots\ldots\ldots\ldots \quad (13)$$

holds. There are generally three contributions to the emittance of a semiconductor: band to band transitions, free carriers, and phonons (lattice vibrations). In the case of defect free crystalline semiconductors such as intrinsic silicon, these three contributions are distinct from one another at low temperatures where the concentration of free carriers is still low. The emissivity increases abruptly when the photon energy exceeds the band gap. An illustration of this phenomenon for the example of intrinsic silicon is given in Fig. 21.[102]

While most of the spectral emissivity analyses have been performed on crystalline semiconductors such as silicon, and other materials such as ceramic films,[102,103] some studies have also been carried out on DLC.[104] Figure 22 shows the transmittance, reflectance, and emittance spectra of DLC produced by PLD; the spectra were measured at a temperature close to room temperature. It can be seen that the emittance spectrum exhibits three regimes (Fig. 22). The first regime corresponds to large wavenumbers (higher photon energies) and shows high emittance. Since DLC films prepared by 248 nm excimer laser with appropriate laser fluence have been reported to

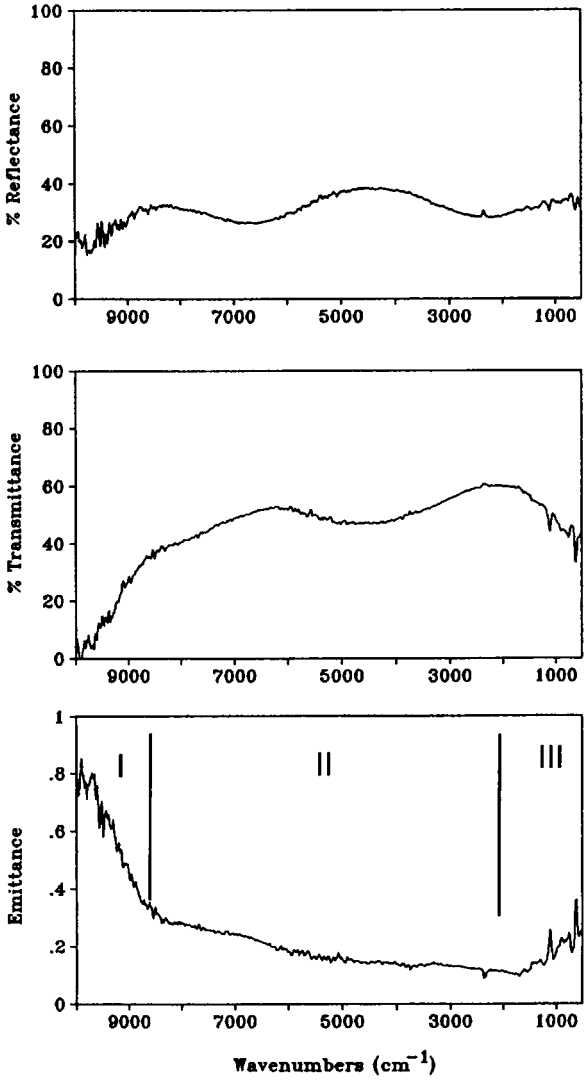

22 Infrared range emissivity measurements of DLC prepared by pulsed laser deposition[104]

have a Tauc gap of $\sim 1{\cdot}0$ eV, with the specific value depending upon the sp^3/sp^2 ratio, the first regime in the transmission spectrum in Fig. 22 may be attributed to the band to band transitions. Apart from this, however, in the case of amorphous semiconductors, there are a large number of localised states, especially close to the band edges. It might be anticipated that these localised states would also contribute to emittance and that they could further smear out the sharp features characteristic of the spectrum of a crystalline material. This is indeed what happens for DLC, where no sharp transitions are observed in the emittance spectrum. Instead, gradual changes are present. The second emissivity regime in Fig. 22 arises from free carriers, while the third regime, of wavelength close to 10 μm, is due to phonon contributions. The emissivity due to free carrier radiation is governed by the impurity concentration of the semiconductor, the thickness of the specimen, and also by the temperature at which the specimen is kept.

X-ray photoelectron spectroscopy of DLC films

In XPS, the energy of the incident photon is large enough to eject electrons from inner cores of atoms.[9] Because energy is conserved when a photon ionises a sample, the energy of the incident photon hv must be equal to the sum of the ionisation energy I of the sample and the kinetic energy of the photoelectron, i.e. the ejected electron

$$hv = \tfrac{1}{2} m_e v^2 + I \quad . \quad . \quad . \quad . \quad . \quad . \quad . \quad . \quad . \quad . \quad . \quad (14)$$

As a first approximation, one would not expect core ionisation energies to be sensitive to the bonds between atoms because they are too tightly bound to be greatly affected by the changes that accompany bond formation. This turns out to be largely true, and the core ionisation energies are characteristic of the individual atoms rather than the overall molecule. Consequently, XPS gives lines characteristic of the elements present in a compound or alloy. For example, the K shell ionisation energy of carbon is 280 eV. However, small shifts of binding energies can be detected and interpreted in terms of the environments of the atoms. This can be used to obtain valuable information about the presence of chemically non-equivalent atoms of the same element.

The XPS technique is mainly limited to the study of surface layers because, even though X-rays may penetrate into the bulk samples, the ejected electrons cannot escape except from within a few nanometres of the surface. Therefore, careful surface preparation of the sample, high vacuum (as high as 10^{-9} torr), and optimised spectrum acquisition time are vital for obtaining meaningful XPS experimental results that can be related to the real conditions of the specimen studied.

Schäfer *et al.*[105] carried out photoemission study of amorphous carbon states (DLC, DLC:H, and a-C:H) and compared the experimental results with calculated DOS values obtained via molecular dynamics simulations. They acquired both the core level (C 1s) XPS spectra and the valence band XPS spectra in order to study the DOS of the various structures. The electronic structures are determined through XPS valence band spectra, which are closely related to the occupied DOS. In crystalline materials the DOS is governed by pronounced structures related to van Hove singularities (where the group velocity of the wave is zero and DOS shows critical points[106]) in the underlying band structure. In amorphous materials the concept of van Hove singularities loses its meaning and the structures in the DOS are usually somewhat more poorly defined than in crystalline materials. Nevertheless, the authors showed a number of striking similarities in the DOS between the amorphous and the two crystalline materials (diamond and graphite), which demonstrate that nearest neighbour, or at least medium range order, in an amorphous material can still be sufficient to produce some of the characteristic features of the corresponding single crystal DOS.

Whether XPS of DLC can give useful information about the specimen, especially the bonding states of the constituents, has been debated in the past. No conclusive agreement has yet been established. It seems that one of the key factors that forbids such attempts is that XPS technique imposes stringent requirements on the surface cleanliness of the specimen, since only the photon induced electrons that are very close to the surface (within a few nanometres) can escape. In the case of DLC, it is difficult to differentiate the contribution from carbon atoms in the surface carbonaceous layer that is universally present. The first few layers of highly tetrahedral DLC films consist of sp^2 carbon.[35,107,108] Schäfer *et al.*,[105] in using XPS to obtain information on bonding states of DLC, based their discussion on a comparison between DLC and surface disordered single crystal diamond (111). In their experimental results, the C 1s core line exhibits a clear asymmetry on the lower binding energy side; typical spectra from this work are shown in Fig. 23. Also, from experiments on clean single crystal diamond (111), a surface core level shift of the C 1s line of $-0{\cdot}82$ eV has been established by Graupner *et al.*[109] Schäfer *et al.* thus argued that, as a zero order approximation, this shift might be taken as representative for sp^2 carbon atoms, though more specific structural properties of a surface reconstruction and relaxation also influence surface core level shifts. They further argued that, by analogy, in the case of sp^3 bonded amorphous carbon these shifts in binding energy would correspond to sp^2 carbon atoms linked mainly by π bonds. Since, as pointed out by Pandey[110] and confirmed recently by Brenner,[111] the clean (111) surface of diamond reconstructs in the form of π bonded chains, this analogy appears to be reasonable. Therefore, as a working hypothesis, Schäfer *et al.*[105] attributed the asymmetry on the low energy side of the C 1s line in the DLC to sp^2 coordinated carbon. Analogous to the XPS experiment on clean single crystal diamond (111), where a surface core level shift of $-0{\cdot}82$ eV of the C 1s line has been established, these authors proposed a hypothesis to ascribe the asymmetry on the low energy side of the C 1s line to sp^2 coordinated carbon. A fit of the C 1s spectrum with two peaks separated by 0·82 eV revealed a percentage of sp^2 contribution that compared well with a value obtained from K edge EELS. Another observation was that the C 1s core lines are approximately twice as wide for the three amorphous

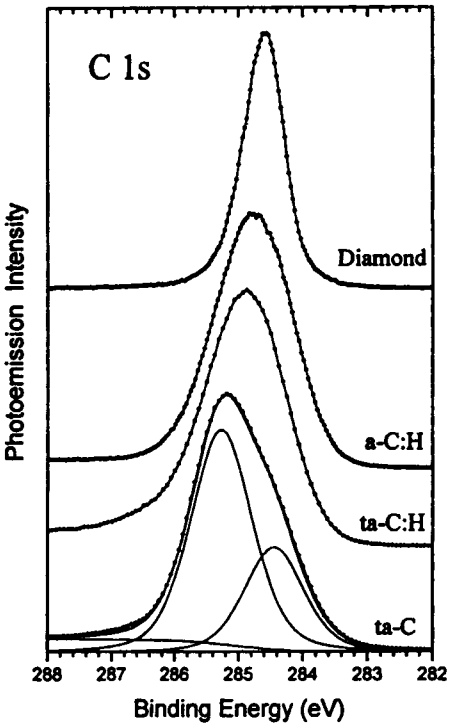

23 X-ray photoelectron spectroscopy of DLC reported by Schäfer *et al.*,[105] showing asymmetry of spectrum for DLC relative to diamond

samples as for diamond, which Schäfer *et al.*[105] ascribe mainly to disorder induced bonding charge fluctuations.

The application of XPS to DLC has not been well acknowledged. This is because there is still some ambiguity in interpreting the spectra. Deconvolution of the entire core level spectra into different components has generated controversy. Furthermore, particularly in the case of DLC, samples are usually cleaned using an ion gun before spectrum acquisition. It is not clear how this process would affect the structure and chemistry of the sample in question. Therefore, interpretation of the spectra needs great care to avoid misleading conclusions.

Electronic properties of DLC films

Electronic properties of DLC have been studied extensively. However, because of the complexity of the system, and especially because of the presence of both sp^3 and sp^2 carbon, complete understanding of this aspect is difficult. As mentioned above, extensive theoretical studies using various methodologies have been reported concerning the atomic structure and vibrational properties of DLC.[58,60,65,66] Theoretical modelling has also been carried out in relation to the electronic structure of DLC. Recently, Robertson has reviewed the electronic structure of DLC[112] and there are about five groups that have carried out detailed electronic structure simulations.[44,58,60,65,92,113–115] Drabold *et al.*[116] emphasised the energy gain from pairing of sp^2 sites to create π bonds, so that one of the two hybridised states is pushed lower in energy and one is pushed higher in energy. Since only the lower energy state is occupied, the total energy is significantly lowered. Further, there is some tendency for the π bonded pairs to form short chains. They found no evidence of rings or cluster formation and argued that the cost in free energy for this to happen would be considerable because of the rather extensive ordering that it would entail. Thus, single sp^2 atoms, or dangling bonds, do not occur in substantial numbers as they do in amorphous silicon. It also appears that defect states associated with geometric anomalies are pushed out of the sp^2 gap into the band edges of the sp^3 gap.

In this section, the electronic behaviour of DLC will be reviewed in the light of its potential applications, starting from electrical transport and subsequently reviewing the very important properties of field emission.

Electrical transport, electronic doping, and related aspects of DLC

It has been found that the optical (Tauc) gap of all types of DLC depends primarily on the sp^2 fraction.[105,112] This is particularly significant at low sp^2 content, where DLC has very rigid networks, yet still has a similar gap.

Another important aspect associated with DLC is the defects, which have certain atomic configurations that give rise to states deep in the band gap. These states are usually more strongly localised than tail states and they act as deep traps for carriers and non-radiative recombination centres. The main defects in σ bonded semiconductors are miscoordinated sites, similar to the three-coordinated dangling bonds in a-Si:H. Dangling bonds also exist in DLC, but the existence of π bonding widens the range of possible defects, so that any cluster with an odd number of sp^2 sites will produce a state near midgap.

Experimental studies on the electronic processes in DLC include photoemission,[27,101] electroconductivity measurements,[117–119] photoconductivity,[41,104,120] and photoluminescence (PL) behaviour,[121,122] dielectric constant measurements,[123,124] electron spin spectroscopy,[112,125] and so on.

Since one of the most promising applications for DLC films is with semiconductor devices, the electric transport, possibility of electronic doping, and mechanism of doping are of tremendous technological interest. Recently, this field has seen some very interesting developments. In the following, the important aspects with respect to theoretical and experimental results are discussed. As stated above, the emphasis will be on hydrogen free diamondlike carbon.

Electrical measurements on DLC have shown that undoped DLC is a p type semiconductor with the Fermi level situated approximately 0·22 eV above the effective valence band edge.[126] Amaratunga *et al.*[125] reported studies on the gap states and discussed the possibility of electronic doping of DLC. The DLC samples were prepared by FCVA and were found to have up to 90% sp^3 bonded carbon. The optical gap of such films is in the range 2·0–2·5 eV. Both theoretical and experimental studies have been conducted on the electronic doping of DLC. It has been doped with phosphorus, nitrogen, and boron.[127–130] It was

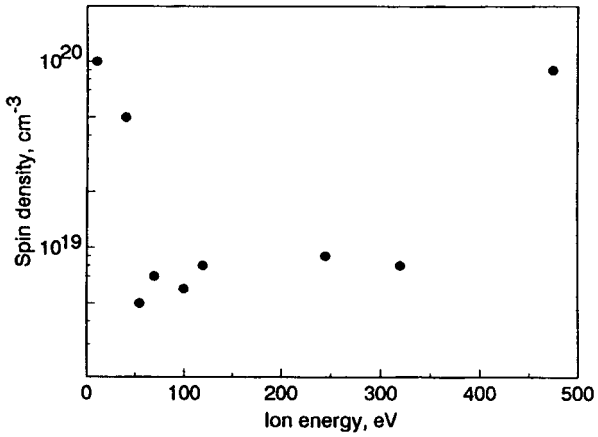

24 Spin density as function of C^+ ion energy for DLC films prepared by filtered cathodic vacuum arc deposition[125]

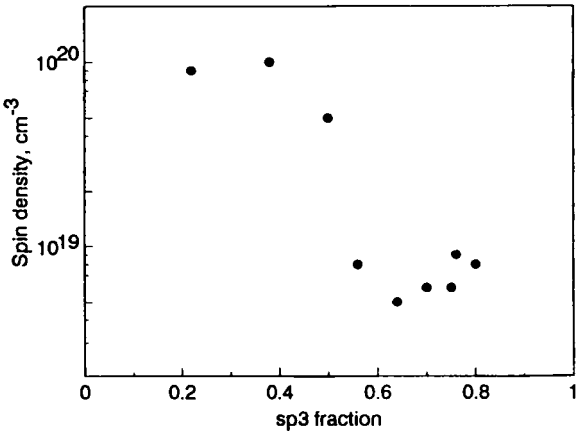

25 Spin density as function of sp^3 fraction for DLC films prepared by filtered cathodic vacuum arc deposition[125]

found that doping allows the room temperature conductivity to be controlled over five orders of magnitude. Unlike a-Si, this doping has been achieved on DLC films containing effectively no hydrogen. In the case of a-Si, in order to achieve electronic doping, hydrogen has to be introduced to passivate the dangling bonds of the random network.[131] Dangling bonds form defect states in the middle of the gap, which act as trap and recombination centres and prevent doping in a-Si. In contrast, DLC can be doped electronically without hydrogen, indicating that it has a sufficiently low density of midgap states. This has been verified by electron spin resonance (ESR) measurements, which detect the unpaired spin in the sample.[125] The spin density has been correlated with the carbon ion energy and the sp^3 fraction. The spin density of DLC made by FCVA is shown as a function of the carbon ion energy in Fig. 24; Fig. 25 depicts the variation of spin density as a function of sp^3 fraction.[125] The spin density passed through a broad minimum as ion energy is increased. When the energy of the carbon ions is less than 25 eV, the spin density is about 10^{20} cm^{-3}, a level typical of hydrogen free a-Si films. An amorphous material with this magnitude of spin density is not a practical electronic material.[125] When the energy is above 40 eV, there is a significant drop in the spin density to around 5×10^{18} cm^{-3} (Fig. 24). It is also observed that the spin density falls rapidly for sp^3 fractions above 40% and then remains roughly constant. It is possible that the lowest spin density occurs when the sp^3 content is 60–70%,[125] rather than at its maximum of 80%.

As a comparison, electronic grade a-Si:H has an unpaired spin density of 10^{16} cm^{-3} (Ref. 131). Therefore the dangling bond density in DLC should be further reduced to improve its use as a semiconductor. However, the fact that DLC possesses low defect density is surprising *per se*, since it has 10–40% sp^2 sites. This suggests that the sp^2 sites do not simply act as isolated dangling bonds, as in a-Si, giving rise to defect gap states, but that they pair up with other sp^2 sites to form π bonding states that lie outside the band gap. Theoretical simulations by Drabold *et al.*[116] and Wang and Ho[66] have given results in accordance with these experimental findings.

Detailed theoretical studies by Stumm *et al.*[130] on the mechanisms of electronic doping of DLC by nitrogen gave very interesting results. They claimed that their 216 atom DLC cell correctly describes the structural and electronic properties of the material. The results confirm their earlier work[65,132] that sp^2 bonded C atoms pair, in agreement with spin density measurements.[125] The electronic DOS also agrees with the experimental results that the gap states are distributed asymmetrically. They found that valence band tail states are spaced closely within a small energy range, while π^* states show a wider energy separation between the tail states. At the same time, the number of localised states in the conduction band tail significantly exceeds that in the valence band tail. In the case of the crystalline counterparts of DLC, computer simulations of substitutional nitrogen incorporation suggest that the Fermi level is moved across the band gap and that the lowest conduction band state therefore becomes occupied. However, these observations cannot be necessarily transferred to DLC: first, because of the high defect density in the gap; and, second, because substitutional nitrogen incorporation is less likely for amorphous materials, since the topological constraints are less severe than in the crystalline lattice.

Results reported in Ref. 130 show that nitrogen atoms do enter the DLC network approximately substitutionally for diamondlike, dangling, π, and weakly stretched bond sites. Some very stretched, or otherwise strongly disordered, bond sites show relaxation around the nitrogen atom that is comparable to the relaxation associated with a nitrogen atom in the diamond lattice (N_3^0). Further, nitrogen incorporation into the network can lead to a graphitisation around the nitrogen atom, such that the nitrogen atom becomes threefold coordinated (N_3^0) and one of its carbon nearest neighbours π bonds to neighbouring, already π bonded, carbon atoms. The total energies for all structures with equal nitrogen concentrations are similar, although dangling bond sites are most energetically favoured. Next most likely is a local rearrangement of the network around the nitrogen atom to form π bonded chains or graphitisation around the nitrogen atom, followed by nitrogen incor-

poration in π bonded sites, diamondlike, and stretched bond sites.

Stumm *et al.*[130] pointed out that considering only the energetics for nitrogen substitution in different sites, most nitrogen atoms are likely to be incorporated in dangling bond sites. Dangling bond sites are energetically most favoured since the former dangling bond midgap state is shifted below the valence band edge when a nitrogen atom is substituted for the carbon dangling bond atom; correspondingly, the Fermi level is lowered. Dangling bond sites are rare in the real material and for typical doping concentrations there are many fewer dangling bond sites than nitrogen atoms. Therefore, on energetic grounds at least, the remaining majority of nitrogen atoms will enter the network in the energetically next favoured, also threefold, coordination. These nitrogen atoms are likely either to promote the formation of graphitic chains without creating an undercoordinated bonding environment (i.e. no dangling bonds appear), or to substitute in π bonded sites. A fourfold bonding environment is energetically least preferred by the nitrogen atom.

This is consistent with the experimental results,[133] where nitrogen dopant concentrations of up to 1% lead to an increase in the sp^2 ratio of the material from about 11 to 25%. The results of Stumm *et al.*[130] for the energetics of various nitrogen substitutions show that this increase in the sp^2 content is in part a result of graphitisation around the nitrogen atom.

The π bonded sites, as well as diamondlike and strained fourfold bonding environments for the nitrogen atoms, are potential doping configurations, since nitrogen incorporation in these sites is mostly substitutional. For nitrogen incorporation in these sites there is little relaxation of the network. No new valence band or gap states are formed and all gap/band tail states remain localised on the same atoms, although the energy of the level may change. Up to a dopant concentration of 2% the Fermi level moves upward by no more than 0·2 eV, as the gap states are filled (Fermi level remains pinned). Increasing the nitrogen concentration in these sites further will eventually compensate all gap states and the Fermi level will move up into the strongly localised conduction band tail states.

Interestingly, the structural and electronic changes for nitrogen in slightly disordered diamondlike sites are different from those for nitrogen in diamond. In diamond, a single nitrogen substitution and moving the nitrogen atom off centre to break the symmetry leads to a relaxation of one of the N–C bonds, such that both the nitrogen atom and one of its carbon nearest neighbours are threefold coordinated. A strongly localised deep trap state is associated with the carbon dangling bond. This relaxation is not present for nitrogen substitution in diamondlike bonds in the DLC structure, even though none of the diamondlike sites in DLC possesses perfect diamond symmetry. Only for very disordered DLC sites does nitrogen substitution result in a relaxation and a corresponding new deep trap state in the conduction band tail. The nitrogen atom enters the lattice at its optimal valence, as determined by the $8-N$ rule,[131] which for nitrogen means threefold coordinated (N_3^0). In this case the Fermi level will move up only to the position of the new defect states created below the conduction band edge.

In order to get conventional effective mass doping in an amorphous material several different criteria have to be met: The nitrogen atom would have to be incorporated not only substitutionally, but also give rise to a donor state fairly close to the conduction band mobility edge. This means that the dopant atom is coordinated such that an electron would occupy the antibonding state if there were no midgap defect states that now take up this electron (compensated doping).

For DLC, most of these requirements are fulfilled and compensated doping takes place. Each substitutionally incorporated nitrogen atom will be in the N_4^+ configuration and donate one electron to occupy gap defect states. Diamondlike relaxations of the network on nitrogen incorporation will initially compensate midgap defect states, until the Fermi level has moved up to the position of the thus newly created defect states in the conduction band tail.

According to Stumm *et al.*,[130] these observations can be categorised into three different mechanisms, all of which will increase the conductivity.

Sitch *et al.*[129] studied boron doping in DLC using a density functional based tight binding method. They compared DLC with diamond. It was found that, in contrast to the diamond case where the acceptor level lies above the top of the σ band, in DLC it lies within the occupied π shoulder that now forms the valence band edge. It is then filled by an electron migrating from a higher energy π state. The Fermi level is consequently pinned by a partially occupied state localised in the π cluster associated with this π state. According to Mott and Davis,[69] there are three mechanisms of conduction in amorphous semiconductors which may be found in appropriate ranges of temperature. They are the following:

(i) transport by carriers excited beyond the mobility edges into non-localised states at E_c or E_v. The conductivity (for electrons) is given by

$$\sigma = \sigma_{min} \exp[-(E_c - E_F)/kT] \qquad (15)$$

a plot of $\ln \sigma$ versus T^{-1} will yield a straight line if $E_C - E_F$ is a linear function of T over the temperature range measured

(ii) transport by carriers excited into localised states at the band edges and hopping at energy close to E_A or E_B. For this process, assuming again conduction by electrons

$$\sigma = \sigma_1 \exp[-(E_A - E_F + w_1)/kT] \qquad (16)$$

where w_1 is the activation energy for hopping conduction

(iii) if the DOS at E_F is finite, then there will be a contribution from carriers with energies near E_F which can hop between localised states by the process analogous to impurity conduction in heavily doped crystalline semiconductors. For this contribution

$$\sigma = \sigma_2 \exp(-w_2/kT) \quad . \quad . \quad . \quad . \quad . \quad . \quad (17)$$

where $\sigma_2 \leqslant \sigma_1$, and w_2 is the hopping energy. At temperatures such that kT is less than the bandwidth, hopping will not be between nearest neighbours and variable range hopping of the form

$$\sigma = \sigma_2' \exp(B/T^{1/4}) \quad . \quad . \quad . \quad . \quad . \quad . \quad . \quad (18)$$

with B a constant depending upon the DOS at E_F, is to be expected, at a temperature sufficiently low for $N(E_F)$ to be considered constant over an energy range $\sim kT$. Equation (18) is the well known Mott–Davis law of conduction for amorphous semiconductors, which has been widely corroborated in many amorphous semiconductor systems.

As pointed out by Sullivan and Friedmann,[117] electronic transport mechanisms in a-C and electronic doping have been the subject of considerable debate. For example, contrary to the work by Stumm *et al.*[130] and Veerasamy *et al.*,[126], Amir and Kalish,[134] Stenzel *et al.*,[135] Ronning *et al.*,[136] and Holmbold *et al.*[137] concluded that incorporation of dopants, specifically phosphorus or nitrogen, into DLC does not give rise to a true doping effect, but instead results in modification of the DOS near E_F or the band edges. Regarding nitrogen doping, however, it has at least been agreed that at high nitrogen concentrations, nitrogen increases the sp^2 fraction, which leads to increased conductivity of the DLC film by increasing the DOS near E_F (or in the band tails), or by increasing the connectivity between the sp^2 sites. This so called microstructural doping of nitrogen has been confirmed by optical absorption and/or EELS measurements[134] and by ultraviolet photoelectron spectroscopy.[138]

The more important problem is nitrogen doping at low concentrations. A threshold concentration of about 1 at.-%N for DLC was reported.[139] However, at least at low fields ($< 10^4$ V cm^{-1}) and near or below room temperature, the conductivity obeys hopping transport.[117] The evidence includes:

(i) low values for the thermal power[134,137]
(ii) conductivity versus temperature measurements that show deviation from models with a single activation energy[137,140]
(iii) current–voltage measurements that show ohmic conduction at low fields and Frenkel–Poole emission at high field[136]
(iv) the observed exponential dependence of conductivity on sp^2 fraction.

Sullivan and Friedman combined stress relaxation and electrical transport studies to identify the transport mechanism in DLC films prepared by PLD.[117] They observed that the conductivity of DLC films is exponentially proportional to increase in threefold carbon concentration (chainlike structure). This result is consistent with thermally activated hopping along carbon threefold chains combined with chain to chain tunnelling. From simple theoretical considerations, they obtained the following equation for calculating the size of the sp^2 chain

$$N = \beta'/\kappa C_0 k_B T \quad . \quad . \quad . \quad . \quad . \quad . \quad . \quad . \quad . \quad . \quad (19)$$

where β' is a parameter that contains the activation energy of conduction, κ is a constant, C_0 is the initial sp^2 fraction, k_B is the Boltzmann constant, and T is absolute temperature. From the experimental data, a typical chain length contributing to the conductivity was estimated to consist of 13 carbon atoms. This value of N is considered to be physically reasonable and is also consistent with the fact that clusters of sp^2 sites are not observed in HRTEM. Thermal annealing at 400°C only increases N from 13 to ~ 14.

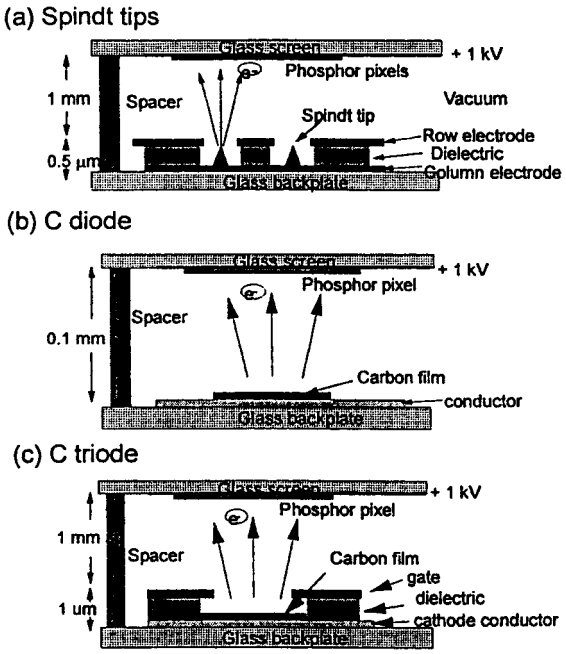

a using molybdenum or silicon Spindt tips; *b* using DLC in diode mode; *c* using DLC in triode mode

26 Schematic illustration of field emission displays[141]

Field emission properties of DLC

One of the most promising applications of DLC is in the flat panel display (FPD), which is now dominated by active matrix liquid crystal displays.[141] However, liquid crystal displays have some disadvantages such as poor viewing angle, high power consumption, and restricted temperature range. An alternative technology is field emission display (FED) and DLC is one of the most interesting candidates to serve this application.[142] Robertson has briefly reviewed the state of the art of studies of DLC associated with applications in FED.[141]

In an FED, electrons are emitted from a matrix of microcathodes and accelerated across a narrow vacuum gap to excite a screen of phosphor pixels. A principal advantage of FEDs is that they retain the high picture quality of cathode ray tubes because they use phosphors with their good brightness, colour contrast, and viewing angle. They are thin, as the electron beam is not scanned, have low power consumption because they use field emission rather than thermionic emission, and are an emissive not subtractive display, so each pixel passes current only when it is on.

Three typical designs of FED are depicted in Fig. 26.[141] The first design (Fig. 26*a*) uses molybdenum or silicon tips as cathodes. The tip radii are

of the order of 20 nm. One of the disadvantages of this mode is that tips can suffer from reliability and lifetime limitations owing to erosion and poisoning. Additionally, the submicrometre size lithography and tip deposition techniques necessary to fabricate these features on large area displays remain prohibitively difficult and expensive for FED applications. An alternative is to use materials which have low electron affinity or even negative electron affinity. These emit electrons at low field. The disadvantages of diamond reside in the fact that diamond deposition requires temperatures exceeding 500°C, which gives rise to thermal budget concerns for microelectronic technologies. Another important point is the graphitic phase in CVD diamond which exists in the grain boundaries and surfaces. To solve these problems, highly sp^3 bonded DLC films, which have a similar bonding environment to diamond, but are synthesised at much lower temperatures, have been widely studied for FED applications, especially in the past five years.[141–144] Two designs for FED using DLC are shown in Fig. 26*b* and *c*.

Recently, Robertson and Rutter reported the band diagram of diamond and DLC surfaces.[143] According to their calculations, DLC has sizeable positive E_A values and the main barrier is at the front surface. Nitrogen is a weak shallow donor that raises the Fermi level to lower the barrier, thus enhancing field emission. It is generally agreed that incorporation of nitrogen will give more effective field emission.[145]

The major concerns associated with FED include breakdown voltage, geometrical uniformity of electron emission, and current density. Figure 27 shows examples of field emission current density and the Fowler–Nordheim plot for DLC and nitrogen doped DLC (DLC:N).[141] It was reported that the emission current was proportional to the number of damaged sites induced by breakdown, implying that the electron emission originated from damaged sites.

The possible application of DLC in FEDs is still a very active area of investigation. More detailed theoretical understanding is still needed.

Mechanical behaviour of DLC films

The mechanical properties of DLC films – elastic modulus, hardness, internal stress, wear resistance, coefficient of friction, etc. – are important for applications such as tribological and antireflective coatings.

Like other properties of DLC, the mechanical properties are governed by the sp^3/sp^2 ratio and chemical composition, e.g. the type and concentration of foreign atoms present in the films. Some properties

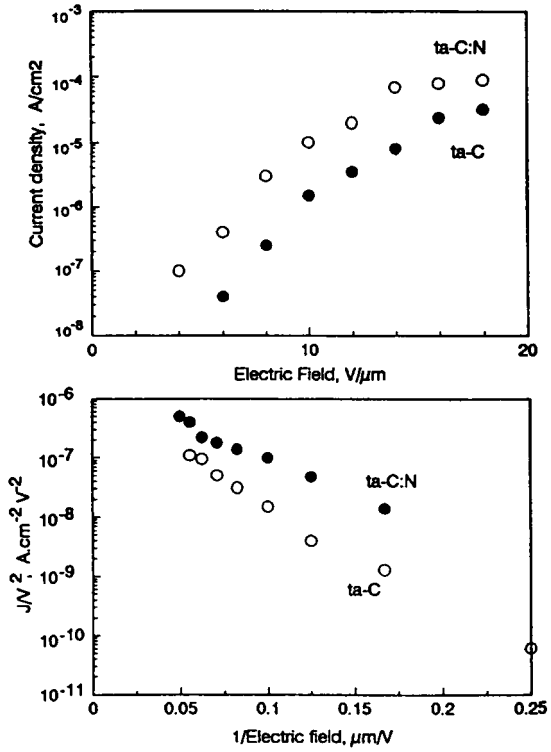

27 Field emission current density and Fowler–Nordheim plot for DLC and DLC:N[141]

of natural diamond and selected DLC films are summarised in Table 4.[52]

Li *et al.*[146] have studied the fracture mechanisms of thin amorphous carbon films in nanoindentation. It was observed that the fracture process takes place in three stages:

(i) ringlike through thickness cracks form around the indenter as a result of high stresses in the contact area
(ii) delamination and buckling are formed around the contact area at the film/substrate interface by the action of high lateral pressure
(iii) further ringlike through thickness cracks and spalling are generated by high bending stresses at the edges of the buckled film.

Based on energy release consideration, the authors further derived an equation to calculate fracture toughness of DLC films from nanoindentation measurements. The fracture toughness is written as

$$K_{IC} = [(E/(1-v^2)2\pi C_R)(U/t)]^{1/2} \quad . \; . \; . \; . \; (20)$$

where E is the elastic modulus of the film, $2\pi C_R$ is the crack length in the film plane, U is the strain

Table 4 Selected properties of natural diamond and selected DLC films[52]

Material	Preparation technique	Density, g cm^{-3}	sp^3, %	Hardness, GPa	Young's modulus, GPa	Friction coeff. against metals
Diamond	Natural	3·52	100	100	1050	0·02–0·10
a-C	Sputtering	1·9–2·4	2–5	11–24	140	0·20–1·20
a-C:H:Me	Reactive sputtering	...	...	10–20	100–200	0·10–0·20
a-C:H	rf plasma	1·57–1·69	...	16–40	145	0·02–0·47
a-C; a-C:H	Ion beam	1·8–3·5	...	32–75	...	0·06–0·19
a-C	Vacuum arc	2·8–3·0	85–95	40–180	500	0·04–0·14
Nanodiamond	PLD	2·9–3·5	75	80–100	300–400	...
a-C	PLD	2·4	70–95	30–60	200–500	0·03–0·12

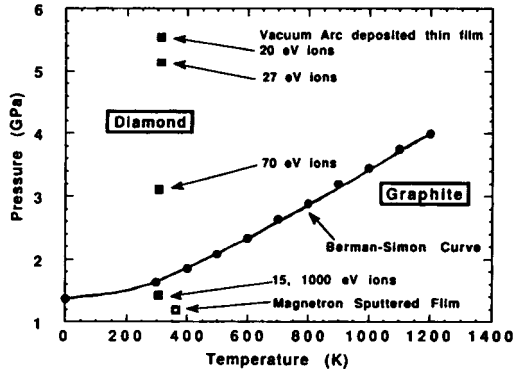

28 Pressure–temperature phase diagram for carbon, showing Berman–Simon curve: solid squares are obtained from measured compressive stresses in vacuum arc deposited films; also shown is the result for a dc magnetron sputtered film[56]

energy difference before and after cracking, and t is the film thickness.

The most serious problem that has plagued the fabrication and application of relatively thick high quality DLC films has been the internal compressive stress that is associated with highly fourfold coordinated DLC films produced by various methods.[40,147,148] Internal stresses as high as 10 GPa have been widely reported, associated with highly tetrahedral DLC. This stress level will unavoidably lead to concerns about adhesion. Therefore, methods to reduce, or even eliminate, the internal compressive stresses in DLC films have long been an important topic for research.

As proposed by McKenzie *et al.*,[56] compressive stress is one of the essential requirements for the formation of highly tetrahedral bonding. This is analogous to the high temperature–high pressure fabrication of diamond, if amorphous tetrahedral carbon is assumed to be the precursor of crystalline diamond, since their physical and chemical features are very close (other than long range order). Figure 28 is the pressure–temperature phase diagram of carbon. It shows the essential conditions for the formation of DLC, as proposed by McKenzie *et al.*[56] This large internal compressive stress gives rise to a serious adhesion problem.

In fact, the term adhesion covers a wide variety of concepts and ideas, depending on whether the subject is discussed from a molecular, microscopic, or macroscopic point of view or whether one talks about formation of the interface or failure of the system. The term adhesion is therefore ambiguous, meaning both the establishment of interfacial bonds and the mechanical load required to break an assembly. Because of this, researchers from different fields of study have proposed many theoretical models of adhesion. These models together are both complementary and contradictory and include:[149,150]

(i) mechanical interlocking
(ii) electronic theory (electrostatic adhesion)
(iii) theory of boundary layers and interphases
(iv) adsorption (thermodynamic) theory
(v) diffusion theory
(vi) chemical bonding theory.

Among these models, it is usually possible to distinguish rather arbitrarily between mechanical and specific adhesion, the latter being based on the various types of bonds (electrostatic, secondary, and chemical) that can develop between two solids. In practice, each of these theoretical considerations is valid to some extent, depending on the nature of the solids in contact and the conditions of formation of the bonded system.

Chemical bonds formed across the coating/substrate interface can greatly contribute to the level of adhesion between materials. These bonds are generally considered as primary bonds, in comparison with physical interactions, such as van der Waals bonding, which are termed secondary force interactions. The terms primary and secondary stem from the relative strength or bond energy of each type of interaction. The typical strength of a covalent bond, for example, is of the order of 100–1000 kJ mol^{-1}, whereas those of van der Waals interactions and hydrogen bonds do not exceed 5·0 kJ mol^{-1}. It is obvious that the formation and strength of chemical bonds depend upon the reactivity of both coating material and substrate material. In the case of thin film deposition *in vacuo*, one of the key parameters that would considerably affect the chemical bonds between the thin film and the substrate is the surface cleanliness of the substrate before deposition and the vacuum condition of the deposition chamber. For instance, if the native oxide of the silicon wafer has not been completely removed before DLC deposition, poor adhesion will usually be observed. On the other hand, fresh silicon surface would usually result in good adhesion since silicon and carbon exhibit strong mutual covalent bonding. This is the reason that some investigators have bombarded the substrate surface with energetic ions such as argon or nitrogen ions to achieve a fresh and chemically active substrate surface.[151]

A direct measure of adhesion may be obtained by applying a force normal to the interface between film and substrate.[152] Tensile tester, ultracentrifuge, and ultrasonic vibration techniques have been utilised to apply the required force, unfortunately with inconsistent results.

An analysis of the forces required to strip the film from the substrate can be conducted following the theoretical consideration by Benjamin and Weaver.[152] At the loads normally used, the substrate surface is drastically deformed at the loaded point. If the substrate is coated with a film, it will be deformed according to the shape of the indentation, causing stretching of the film and the development of a shearing force between the film and the substrate surface. This shearing force would have a maximum value at the tip of the indentation, and the tensile forces in the film would be small in comparison. When the critical load is reached, the shearing force in the film would be sufficient to break the adhesive bonds between film and substrate. At higher loads, the motion of the indentor would plough the film aside and leave a clear channel.

Adhesive failure of thin films occurs when the internal stress σ exceeds a critical value. A film of

thickness h delaminates when the mechanical energy density exceeds the energy needed to create two new surfaces, i.e.[153]

$$2G_1[(1+v)/(1-v)]hf^2 < 2\gamma \quad . \quad . \quad . \quad . \quad . \quad . \quad . \quad (21)$$

where γ is the surface/interfacial energy, v the Poisson's ratio, G_1 the shear modulus of the film, and f the strain in the film. Writing the equation in terms of strain gives

$$h < (\gamma/G_1 f^2)[(1-v)/(1+v)] \quad . \quad . \quad . \quad . \quad . \quad . \quad . \quad (22)$$

This equation sets an upper limit on film thickness. Thus stated, a film of certain thickness would bulge when the mechanical energy density exceeds the energy required to create two fresh surfaces.

An indicator of the large internal compressive stress in a film is the buckling pattern of stress release. The buckling patterns found in DLC films have long been recognised.[154] The buckling of DLC exhibits a typical sinusoidal shape and can be treated theoretically by adopting the methodology developed for thin shells. The sinusoidal buckling patterns indicate clearly that they arise as a result of the relief of compressive stress in the film.

Usually, the Stoney formula can be used to calculate the internal stress of a thin film system. This equation can be written as

$$\sigma_f = (6R)^{-1}(E_s d_s^2)/(1-v_s)d_f \quad . \quad . \quad . \quad . \quad . \quad . \quad . \quad (23)$$

where R is the radius of curvature of the system due to stress, E_s is the Young's modulus of the substrate, d_s is the thickness of the substrate, v_s is the Poisson's ratio of the substrate, and d_f is the thickness of the film. Values of σ_f are determined through measurement of R by means of techniques such as interference fringe and beam deflection.[155]

An alternative way of measuring the internal stresses of DLC films is by measuring the Raman peak shift. In this method, the G peak shifts are usually measured and compared against a stress free reference sample. Raman spectroscopy has been used to probe the stress–strain conditions of materials with quite consistent results.[156,157] This is because of the fact that the stress–strain dependent property, the frequency of the atomic vibrations in a material, can be characterised by laser Raman spectroscopy. The principle by which this technique works is that when a material is stressed, the equilibrium separation between its constituent atoms is altered in a reversible manner. As a result, the interatomic force constants that determine the atomic vibrational frequencies also change since they are related to the interatomic separation. In general, as the bond lengths increase with tensile load, the force constants and, hence, the vibrational frequencies decrease, whereas the reverse effect is present when the material is subjected to hydrostatic or mechanical compression. This effect has universal applicability in materials as diverse as commercial polymers, amorphous phases, or inorganic materials such as silicon.

Accordingly, the magnitude of the Raman shift can be related to the residual stress σ by the equation

$$\sigma = 2G[(1+v)/(1-v)](\Delta\omega/\omega_0) \quad . \quad . \quad . \quad . \quad . \quad (24)$$

where $\Delta\omega$, ω_0, G, and v are the shift in the Raman wavenumber, the wavenumber of a reference state (not necessarily the stress free state), the shear modulus of the material, and the Poisson's ratio of the material respectively.

Detailed analysis can be carried out on the visible Raman data since the Raman spectra can generally be resolved into two Gaussians to achieve the best possible fit. However, the peak positions may be different from those obtained via ultraviolet Raman spectroscopy, since different experimental routes are used in that case. Ager *et al.*[158] have studied the effect of intrinsic growth stress on the Raman spectra of FCVA deposited amorphous carbon films. They controlled the magnitude of the stress by changing the incoming energy of the ions. It is observed that compressive stress shifts the Raman scattering feature in the films to higher frequency by as much as $20\ cm^{-1}$. They used the Raman spectra of adhering and delaminated films to measure the magnitude of the stress induced shift, and obtained a value of $-1{\cdot}9\ cm^{-1}\ GPa^{-1}$ for compressive biaxial stress.

Traditional approaches to obtain DLC films with low internal stress levels involve increasing deposition temperatures or decreasing the energies of carbon species arriving at the substrate surface, etc. Unfortunately, all these are achieved at the expense of reducing sp^3/sp^2 ratio and thus result in poor quality films. Therefore, this has become a seemingly insurmountable stumbling block for the applications of thick DLC films. Wei *et al.*[159–163] have presented both visible and ultraviolet Raman spectra of some DLC films that are either dopant free or contain foreign atoms such as copper, titanium, or silicon. They observed the trend that the presence of dopant leads to shift of the G peak to smaller wavenumber, indicating that the internal compressive stress of the films is decreased. They used pure DLC as the reference, and used the mechanical properties of DLC as measured by nanoindentation to calculate the internal stress reduction according to equation (24).

Sullivan and co-workers[148,164] reported the stress relaxation and thermal evolution of film properties for highly tetrahedrally bonded amorphous carbon. They proposed a model for the stress relaxation. The onset of stress relaxation in these materials occurs following thermal annealing at temperatures as low as 100°C, and near full stress relaxation occurs after annealing at 600°C. The stress relaxation is modelled by a series of first order chemical reactions which lead to a conversion of some fourfold coordinated carbon atoms into threefold coordinated carbon atoms. Anders *et al.*[165] reported similar studies on thermal stability of amorphous hard carbon films produced by cathodic arc deposition. They characterised the films by near edge X-ray absorption fine structure (NEXAFS) spectroscopy, Raman spectroscopy, and nanoindentation. Figure 29 shows the NEXAFS spectra of the films deposited by Anders *et al.*[165] The DLC films were heated to different temperatures in ultrahigh vacuum. It can be seen that no change appears in the spectral characteristics on annealing at up to 700°C, and a weak graphitic exciton peak appears at 292 eV at annealing temperatures of 800 and 850°C. The hardness and elastic modulus of the as deposited and annealed (at 850°C

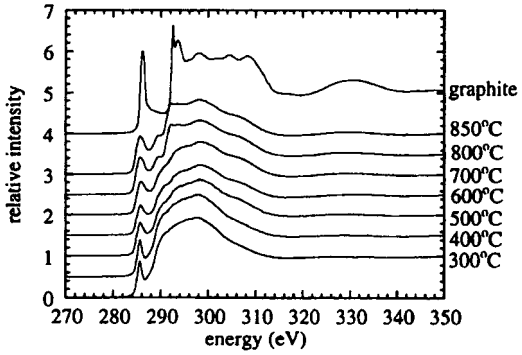

29 Near edge X-ray absorption fine structure spectra of cathodic arc deposited amorphous hard carbon film heated at various temperatures in ultrahigh vacuum: weak graphitic exciton peak appears at 292 eV at annealing temperatures of 800 and 850°C[165]

in vacuum) amorphous carbon films are shown in Fig. 30. Again no change is observed after annealing.

A more recent and more detailed investigation on the stress reduction and bond stability during annealing of DLC is due to Ferrari *et al.*[166] They observed complete stress relief after annealing at 600–700°C, which is accompanied by minimal structural modifications, as indicated by EELS, ultraviolet and visible Raman spectroscopy, and optical gap measurements. The stress reduction as a function of annealing time for samples annealed in a nitrogen furnace at various temperatures is illustrated in Fig. 31 and the sp^3 fraction from EELS measurements as a function of annealing temperature in Fig. 32. The striking feature of the latter figure is the retention of the bond structure of the DLC films after high temperature annealing (up to 1000°C). Both visible and ultraviolet Raman scattering measurements yield consistent results.

Though further theoretical and experimental studies on stress reduction by thermal annealing may still be needed, these studies may have paved the way to fabrication of stress free, high quality, thick DLC films.

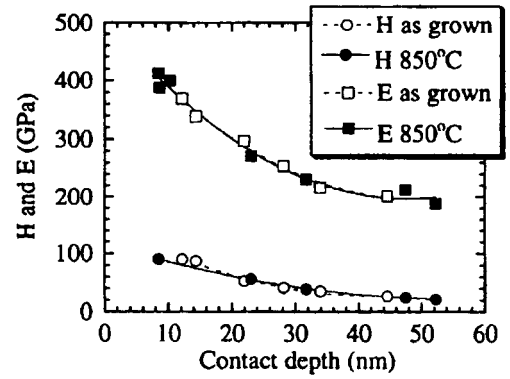

30 Nanohardness (*H*) and elastic modulus (*E*) of cathodic arc deposited hard amorphous carbon films as function of indentation depth before and after annealing up to 850°C: no change is observed after annealing[165]

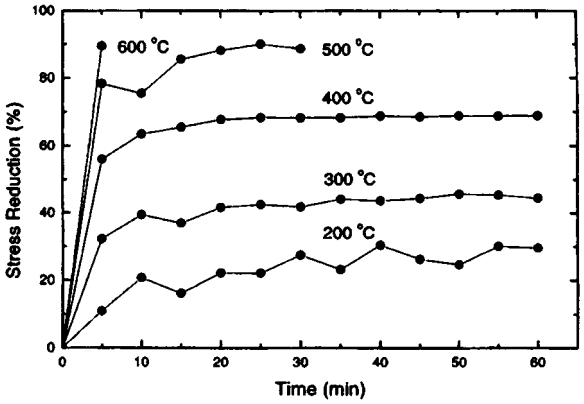

31 Stress relief as function of annealing time for samples furnace annealed in nitrogen at various temperatures[166]

Monteiro *et al.*[167] achieved significant internal stress reduction in DLC films doped with titanium and tungsten. The films were produced by a dual source vacuum arc plasma immersion technique. The authors also found evidence of nanocrystal TiC and WC in HRTEM studies. This would not be surprising in view of the film preparation technique used.

Dorfman has reviewed investigations of diamondlike nanocomposites (DLN).[168] The structure of these thin film composites consists of atomic scale composite random networks of carbon and silicon. The carbon network is stabilised by hydrogen and the silicon network is stabilised by oxygen. The mutual stabilisation of these interpenetrating atomic scale filaments and the common random network structure prevents the growth of graphitic carbon at high temperature, serving to enhance adhesion and reduce the internal stress in these films. Such self-stabilised C–Si amorphous structures form a matrix for the introduction of metals. These metals are distributed as separate atoms or as separate disordered networks, and all three networks (the carbon matrix, a-Si, and a-Me) are bonded together. It was found that diamondlike properties and the structure are preserved in both metallic and dielectric states.

In the past, some efforts have been directed toward improving the adhesion of DLC films by depositing

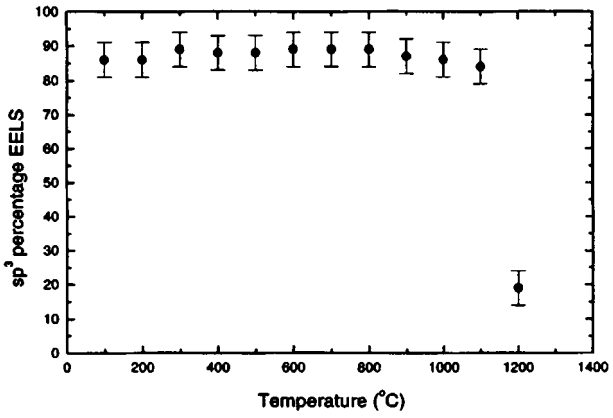

32 Retention of sp^3 fraction as function of annealing temperature for cathodic arc deposited DLC films[166]

an interlayer between the DLC film and the substrate or producing multilayer structure.[169–175] For example, Bentzon *et al.*[170] used metallic interlayers to study the enhancement of the adhesion of DLC on steel. It was found that Cu/Cr appeared to provide the best adhesion. However, the authors did not provide convincing evidence for their observations, in light of the fact that there is weak chemical bonding between carbon and copper, which leads to poor adhesion of diamond films to copper substrates. Therefore, a better understanding of the mechanism of improvement of adhesion through metallic interlayers needs to be developed. A possible mechanism may be related to the accommodation of the compressive stress by copper to provide stress relief in DLC films, thus copper providing a compliant layer.

Recently, functionally graded and nanolayered DLC coatings have been successfully fabricated by a combined used of pulsed laser deposition and magnetron sputtering.[176] In addition to the improvement in adhesion, the toughness of the films was found to be significantly enhanced. Coatings grown using this approach had a gradual transition of chemistry, structure, and properties from substrate material to DLC, without producing sharp interfaces which are considered to be potential sites for crack initiation. The fabrication of functionally graded DLC coatings includes the formation of an adhesive thin metal layer, transition to a load supporting carbide layer, the addition of a metal doped DLC layer, and subsequent deposition of multiple pairs of metal/DLC or carbide/DLC layers.[177,178] Graded transitions of coating properties across the thickness without the presence of sharp interfaces considerably improved the coating response to high contact load. For a single layer coating, a surrounding peripheral crack and large areas of delamination alongside the scratch path were characteristic failures, which occurred at contact loads $\geqslant 15$ N. In contrast, the functionally graded coating underwent neither peripheral cracking nor adhesion failure until the diamond stylus penetrated the substrate at loads close to 50 N.

Since DLC thin coatings have been used as protective coatings for magnetic disk drives, the tribological performance of DLC and its dependence on sp^3/sp^2 ratio have been studied extensively.[42,57,179–181] It is usually recognised that DLC thin films have very low coefficient of friction ($<0{\cdot}1$) and the wear resistance is a strong function of atmosphere as well as the film quality, particularly the sp^3/sp^2 ratio. One of the major advantages of DLC films over polycrystalline diamond thin films is that DLC films are usually extremely smooth. A study on the effect of diamondlike carbon coating and surface topography on the performance of metal evaporated magnetic tapes showed that DLC coating prevented catastrophic abrasive wear and reduction in head to tape spacing or intimate contact during cycling tests, but could not significantly improve the durability of the tape.[182] Coating with DLC reduces asperity compliance compared with uncoated tapes. In pause mode, DLC coating improved magnetic reliability and tribological performance by preventing the heads from contacting the metallic magnetic layer. The authors proposed, on the basis of their studies, that a flat tape must be used for magnetic considerations and DLC coating is needed to prevent abrasive wear and intimate contact.

Applications of DLC and associated problems

Current commercialised application of DLC thin coatings includes microtribology in the microelectronics industry.[42,182] Potential applications under exploration include flat panel displays, biomedical devices,[180,183] and electronic devices.[184,185]

Medical applications of DLC include surface engineering of replacement human body joints such as hip or knee joints. It is usually realised that the tribochemical conditions, e.g. in a hip joint, are very severe; even the best materials, such as the Co–Cr–Mo alloys that are used currently, are dissolved or wear by at least 0·02–0·06 mm in 10 years (mean linear wear rate). Much effort has been expended in developing hard, biocompatible coatings with a sufficiently low coefficient of friction to improve the performance of artificial joints. Lappalainen *et al.*[180] reviewed some relevant issues related to the use of DLC coatings for medical applications. They deposited DLC films (sp^3 fraction $\sim 80\%$, coating thickness 200–1000 nm) on Co–Cr–Mo alloy, stainless steel, titanium alloy (Ti–6Al–4V), and alumina test samples and hip and knee joints using a pulsed plasma accelerator method. It was shown that, by using high energy plasma beams and proper intermediate layers, the adhesion of the DLC coatings can be greatly improved. These DLC coatings are biocompatible, causing no local tissue reactions, and offer good tribological characteristics. The issues discussed include:

(i) good adhesion of the coating to the implant surface and the production of high quality coatings
(ii) the need for a high quality surface finish
(iii) the need for good corrosion resistance in biological fluids.

Lappalainen *et al.*'s results show that, in all the combinations studied, DLC coating gave an improvement in wear and corrosion resistance compared with the uncoated materials. In the best cases, the wear rate was decreased by a factor of 30–600.

Recently, Gerstner and McKenzie reported the fabrication and characterisation of novel electronic devices using DLC doped with nitrogen.[185] Rather than trying to reduce the trap states in the mobility gap, they made use of them as a means of producing non-volatile digital information storage devices. The devices were made by depositing DLC:N films on aluminium films that had been thermally evaporated on both glass and polished silicon substrates, and contacting the top of the DLC with an inner sprung gold point contact. They acquired current–voltage characteristics under various conditions and observed a memory effect in through film current–voltage characteristics taken between an underlying aluminium film, using a gold point contact either side of the DLC:N film. A kink was observed when increasing the bias in the positive direction, as shown in Fig. 33. When the voltage was swept in the opposite direction, the kink disappeared. Gerstner and McKenzie also

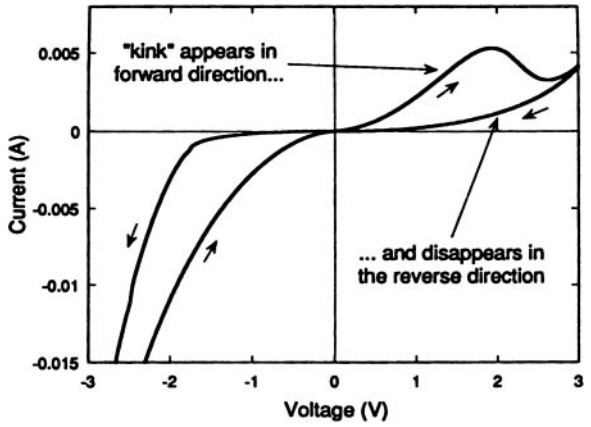

33 Through film *I–V* characteristics of DLC:N thin film between planar and point electrodes (with sign referring to bias of point contact):[185] arrows indicate direction of voltage sweep (sweep rate = 0·83 V s^{-1})

found that the kink occurred only after the application of negative biases beyond a certain threshold (around −2·5 V), and disappeared after the application of a positive bias beyond a similar threshold (around +2·5 V).

The kink phenomenon was found to increase both with the duration of the application of negative bias (*see* Fig. 34) and with increasing film thickness (*see* Fig. 35). This suggests that the effect is a bulk effect, not related to the possible presence of an oxide at the aluminium/carbon interface. Based on their preliminary experimental work, Gerstner and McKenzie proposed that new possibilities exist for utilisation of the high trap densities present in DLC. Thus, new interest may be kindled for further investigation of the effects of donor traps on the electronic properties of DLC and other amorphous semiconductors, and in their potential use in novel device applications.

Concluding remarks

Diamondlike carbon (DLC) or tetrahedral amorphous carbon (ta-C) is the amorphous state of carbon

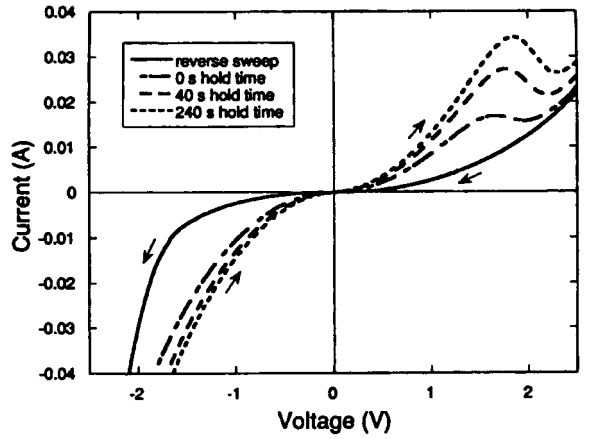

34 Effect of holding device for given amount of time before collection of complete *I–V* characteristic (sweep rate = 0·83 V s^{-1}):[185] characteristic in opposite direction (solid line) is also shown

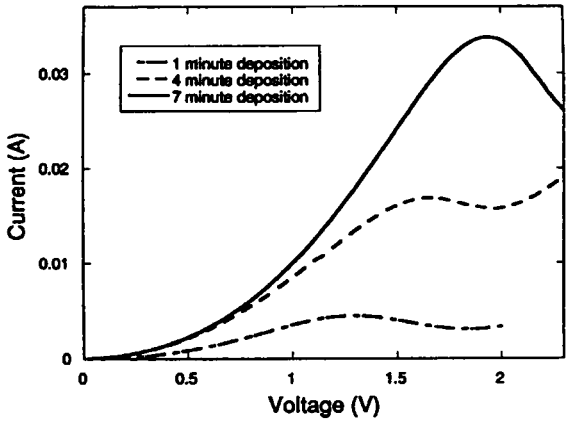

35 Effect of DLC:N film thickness on size of kink in forward *I–V* characteristics (sweep rate = 0·83 V s^{-1})[185]

mainly consisting of sp^3 carbon atoms. It is one of the many interesting forms of carbon that raise important theoretical questions and have enormous possibilities for practical applications. If properly prepared, DLC can have properties that rival those of crystalline diamond. Coatings of DLC can possess properties close to diamond in terms of elastic modulus, hardness, atomic smoothness, infrared transparency, and chemical inertness. The beneficial properties of DLC stem from the continuous rigid random networks of sp^3 atoms, and the properties can essentially be tailored within a wide spectrum by controlling the sp^3/sp^2 ratio. Thin film deposition techniques that have been successfully used to prepare high quality DLC coatings include pulsed laser ablation (PLA), filtered cathodic vacuum arc (FCVA) deposition, and mass selected ion beam (MSIB) deposition, with the last two techniques having been initially invented for deposition of pure, high quality superhard DLC coatings. In the past decade, tremendous progress has been witnessed in experimental and theoretical investigations of hydrogen free DLC. Experimental and commercial applications in microelectronics, microtribology, biomedical technologies, and so on have been demonstrated. Potential applications include sensors, flat panel displays, and photodiodes. Study of the various aspects of DLC has been and will be a very active field.

Acknowledgements

This research project was sponsored by the National Science Foundation under contract CMS9414434.

References

1. P. BALL: *Nature*, 8 Jan. 1998, **391**.
2. K. E. SPEAR: *J. Am. Ceram. Soc.*, 1989, **72**, 171.
3. H. W. KROTO, J. R. HEATH, S. C. O'BRIEN, R. F. CURL, and R. E. SMALLEY: *Nature*, 1985, **318**, 162; recent advances in this field may be found in H. KUZMAMY, J. FINK, M. MEHRING and S. ROTH (eds.): 'Fullerenes and fullerene nanostructures'; 1996, Singapore, World Scientific and P. BERNIER, D. S. BETHUNE, L. Y. CHIANG, T. W. EBBESEN, R. M. METZGER, and J. W. MINTMIRE (eds.): 'Science and technology of fullerene materials', Symp. Proc. 359; 1995, Warrendale, PA, MRS.
4. T. W. EBBESEN (ed.): 'Carbon nanotubes: preparation and properties'; 1997, Baton Rouge, LA, CRC Press.

5. S. IIJIMA: *Nature*, 1991, **354**, 56.
6. M. L. COHEN: *Phys. Rev. B*, 1985, **B32**, 7988.
7. P. DLANEY, H. J. CHOI, J. IHM, S. G. LOUIE, and M. L. COHEN: *Nature*, 1998, **391**, 466.
8. J. KRISHNASWAMY, A. RENGAN, J. NARAYAN, K. VEDOM, and C. J. McHORGUE: *Appl. Phys. Lett*., 1989, **54**, 2455.
9. P. W. ATKINS: 'Physical chemistry', 5th edn; 1994, Basingstoke, W. H. Freeman.
10. J. ROBERTSON: *Prog. Solid State Chem*., 1991, **21**, 199.
11. J. ROBERTSON: *Adv. Phys*., 1986, **35**, 317–374.
12. J. ROBERTSON: *Mater. Sci. Forum*, 1990, **52–53**, 125–150.
13. S. R. P. SILVA *et al*. (eds.): 'Amorphous carbon: state of the art'; 1998, Singapore, World Scientific.
14. J. W. MOORE: 'Basic physical chemistry'; 1983, Englewood Cliffs, NJ, Prentice Hall.
15. S. AISENBERG and R. CHABOT: *J. Appl. Phys*., 1971, **42**, 2953.
16. D. NIR, R. KALISH, and G. LEVIN: *Thin Solid Films*, 1984, **117**, 125.
17. A. GRILL, B. MEYERSON, V. PATEL, J. REIMER, and M. PETRICH: *J. Appl. Phys*., 1987, **61**, 2874.
18. O. MATSUMOTO, H. TOSHIMA, and Y. KANZAKI: *Thin Solid Films*, 1985, **128**, 341.
19. I. G. BROWN: *Ann. Rev. Mater. Sci*., 1998, **28**, 243–269.
20. N. SAVVIDES and B. WINDOW: *J. Vac. Sci. Technol. A*, 1985, **A3**, 2386.
21. J. KULIK, Y. LIFSHITZ, G. D. LEMPERT, J. W. RABALAIS, and D. MARTON: *J. Appl. Phys*., 1994, **76**, 5063.
22. S. AISENBERG and F. M. KIMOCK: *Mater. Sci. Forum*, 1990, **52–53**, 1–40.
23. H. R. KAUFMAN, J. J. CUOMO, and J. M. E. HARPER: *J. Vac. Sci. Technol*., 1982, **21**, 725–736.
24. S. AISENBERG and R. CHABOT: *J. Vac. Sci. Technol*., 1973, **10**, 104.
25. P. KOIDL, C. WILD, B. DISCHLER, J. WAGNER, and M. RAMSTEINER: *Mater. Sci. Forum*, 1989, **52–53**, 41.
26. Y. LIFSHITZ, S. R. KASI, and J. W. RABALAIS: *Mater. Sci. Forum*, 1989, **52–53**, 237–290.
27. Y. LIFSHITZ *et al*.: *Diam. Relat. Mater*., 1997, **6**, 687.
28. S. CHRISTIANSEN, M. ALBRECHT, G. FRANK, H. P. STRUNK, C. RONNING, H. HOFSASS, and E. RECKNAGEL: *Diam. Relat. Mater*., 1998, **7**, 15–22.
29. B. F. COLL, P. SATHRUM, R. AHARONOV, and M. A. TAMOR: *Thin Solid Films*, 1992, **209**, 165–173.
30. M. CHHOWALLA, Y. YIN, G. A. J. AMARATUNGA, D. R. MCKENZIE, and Th. FRAUENHEIM: *Diam. Relat. Mater*., 1997, **6**, 207.
31. V. S. VEERASAMY, J. YUAN, G. A. AMARATUNGA, W. I. MILNE, K. W. R. GILKES, M. WEILER, and L. M. BROWN: *Phys. Rev. B*, 1993, **B48**, 17954–17959.
32. P. J. MARTIN, S. W. FILIPCZUK, R. P. NETTERFIELD, J. S. FIELD, D. F. WHITALL, and D. R. McKENZIE: *J. Mater. Sci. Lett*., 1988, **7**, 410.
33. C. A. DAVIS, V. S. VEERASAMY, G. A. J. AMARATUNGA, W. I. MILNE, and D. R. McKENZIE: *Philos. Mag. B*, 1994, **B69**, 1121–1131.
34. I. I. AKSENOV, V. G. PADALKA, V. T. TOLOK, and V. M. KOROSHIH: *Sov. J. Plasma Phys*., 1980, **6**, (4), 504–507.
35. G. M. PHARR, D. L. CALLAHAN, S. D. McADAMS, T. Y. TSUI, S. ANDERS, A. ANDERS, J. W. AGER III, I. G. BROWN, C. S. BHATIA, S. R. P. SILVA, and J. ROBERTSON: *Appl. Phys. Lett*., 1996, **68**, (6), 779–781.
36. W. I. MILNE: *J. Non-Cryst. Solids*, 1996, **198–200**, 605.
37. R. LOSSY, D. L. PAPPAS, R. A. ROY, and J. J. CUOMO: *Appl. Phys. Lett*., 1992, **61**, 171.
38. J. J. CUOMO, J. P. DOYLE, J. BRULEY, and J. C. LIU: *J. Vac. Sci. Technol. A*, 1991, **A9**, 2210.
39. D. B. KERWIN, I. L. SPAIN, R. S. ROBINSON, B. DAUDIN, M. DUBUS, and J. FONTENILLE: *Thin Solid Films*, 1987, **148**, 311–321.
40. D. NIR: *Thin Solid Films*, 1987, **146**, 27.
41. B. ANDRE, F. ROSSI, A. van VEEN, P. E. MIJNARENDS, H. SCHUT, and M. P. DELPLANCKE: *Thin Solid Films*, 1994, **241**, 171–174.
42. A. KOBAYASHI, D. YOSHITOMI, O. YOSHIHARA, T. IMAYOSHI, A. KINBARA, T. FUMOTO, and M. UENO: *Surf. Coat. Technol*., 1995, **72**, 152–156.
43. M. GIOTI and S. LOGOTHETIDIS: *Diam. Relat. Mater*., 1998, **7**, 444–448.
44. R. K. SINGH, D. H. LOWNDES, D. B. CHRISEY, E. FOGARASSY, and J. NARAYAN (eds.): 'Advances in laser ablation of materials', Symp. Proc. 526; 1998, Warrendale, PA, MRS.
45. R. K. SINGH, O. W. HOLLAND, and J. NARAYAN: *J. Appl. Phys*., 1990, **68**, (1), 233–247.
46. R. K. SINGH and J. NARAYAN: *Phys. Rev. B*, 1990, **B41**, 8843.
47. A. A. VOEVODIN, S. D. WALCK, J. S. SOLOMON, P. J. JOHN, D. C. INGRAM, M. S. DONLEY, and J. S. ZABINSKI: *J. Vac. Sci. Technol. A*, 1996, **14A**, 1927.
48. E. A. ROHLFING: *J. Chem. Phys*., 1998, **89**, (10), 6103–6112.
49. J. A. GREER and M. D. TABAT: *J. Vac. Sci. Technol. A*, 1995, **13A**, 1175.
50. S. S. WAGAL, E. M. JUENGERMAN, and C. B. COLLINS: *Appl. Phys. Lett*., 1988, **53**, 187.
51. D. R. TALLANT, T. A. FRIEDMANN, N. A. MISSERT, M. P. SIEGAL, and J. P. SULLIVAN: in 'Covalently bonded disordered thin-film materials', (ed. M. P. Siegal *et al*.), Symp. Proc. 498 37; 1997, Warrendale, PA, MRS.
52. A. A. VOEVODIN and M. S. DONLEY: *Surf. Coat. Technol*., 1996, **82**, 199.
53. Y. YAMAGATA, A. SHARMA, J. NARAYAN, R. M. MAYO, J W. NEWMAN, and K. EBIHARA: *J. Appl. Phys*., 1999, **86**, 4154.
54. H.-J. SCHEIBE, B. SCHULTRICH, and D. DRESCHER: *Surf. Coat. Technol*., 1995, **74–75**, 813–818.
55. P. SIEMROTH and H.-J. SCHEIBE: *IEEE Trans. Plasma Sci*., 1990, **18**, 911–916.
56. D. R. McKENZIE, D. MULLER, and B. A. PAITHORPE: *Phys. Rev. Lett*., 1991, **67**, 773.
57. X. L. PENG and T. W. CLYNE: *Diam. Relat. Mater*., 1998, **7**, 944–950.
58. D. BEEMAN, J. SILVERMAN, R. LYNDS, and M. R. ANDERSON: *Phys. Rev. B*, 1984, **30**, 870.
59. D. E. POLK: *J. Non-Cryst. Solids*, 1971, **5**, 365.
60. P. STEINHARDT, R. ALBEN, M. G. DUFFY, and D. E. POLK: *Phys. Rev. B*, 1973, **B8**, 6021.
61. J. ROBERTSON and E. P. O'REILLY: *Phys. Rev. B*, 1987, **B35**, 2946–2957.
62. J. SCHWAN, S. ULRICH, T. THEEL, H. ROTH, H. EHRHARDT, P. BECKER, and S. R. P. SILVA: *J. Appl. Phys*., 1997, **82**, (12), 6024–6030.
63. J. TERSOFF: *Phys. Rev. B*, 1991, **B44**, 12039.
64. P. A. GASKELL, A. SAEED, P. CHIEUX, and D. R. McKENZIE: *Phys. Rev. Lett*., 1991, **67**, 1286.
65. D. A. DRABOLD, P. A. FEDDERS, and P. STUMM: *Phys. Rev. B*, 1994, **B49**, 16415.
66. C. Z. WANG and K. M. HO: *Phys. Rev. Lett*., 1993, **71**, 1184.
67. R. TUINSTRA and J. L. KOENIG: *J. Chem. Phys*., 1970, **53**, 1126–1130.
68. R. J. NEMANICH, J. T. GLASS, G. LUCOVSKY, and R. E. SHRODER: *J. Vac. Sci. Technol. A*, 1988, **A6**, 1783.
69. N. F. MOTT and E. A. DAVIS: 'Electronic processes in non-crystalline materials', 2nd edn; 1979, Oxford, Clarendon Press.
70. A. YOSHIMORI and Y. KITANO: *J. Phys. Soc. Jpn*, 1956, **2**, 352.
71. J. A. YOUNG and J. U. KOPPEL: *J. Chem. Phys*., 1965, **42**, 357.
72. R. SHUKER and R. W. GAMMON: *Phys. Rev. Lett*., 1970, **25**, 222–225.
73. C. C. TSAI and R. J. NEMANICH: *J. Non-Cryst. Solids*, 1980, **35–36**, 1203.
74. J. WAGNER, M. RAMSTEINER, Ch. WILD, and P. KOIDL: *Phys. Rev. B*, 1989, **B40**, 1817–1824.
75. M. YOSHIKAWA, G. KATAGIRI, H. ISHIDA, A. ISHITANI, and T. AKAMATSU: *Solid State Commun*., 1988, **66**, 1177–1180.
76. J. WAGNER, C. WILD, and P. KOIDL: *Appl. Phys. Lett*., 1991, **59**, 779.
77. M. RAMSTEINER, J. WAGNER, Ch. WILD, and P. KOIDL: *Solid State Commun*., 1988, **67**, 15–18.
78. A. V. STANISHEVSKY, L. Yu. KHRIACHTCHEV, R. LAPPALAINEN, and M. RASANEN: *Diam. Relat. Mater*., 1997, **6**, 1026–1030.
79. M. A. TAMOR and W. C. VASSELL: *J. Appl. Phys*., 1994, **76**, 3823.
80. S. PRAWER, K. W. NEGENT, Y. LIFSHITZ, G. D. LEMPERT, E. GROSSMAN, J. KULIK, I. AVIGAL, and R. KALISH: *Diam. Relat. Mater*., 1996, **5**, 433–438.
81. J. D. HUNN, S. P. WITHROW, and C. W. WHITE: *Phys. Rev. B*, 1995, **B52**, 8106.
82. V. PAILLARD, P. MÉLINON, V. DUPUIS, A. PEREZ, J. P. PEREZ, G. GUIRAUD, J. FORNAZERO, and G. PANCZER: *Phys. Rev. B*, 1994, **B49**, 11433.
83. V. I. MERKULOV, J. S. LANNIN, C. H. MUNRO, S. A. ASHER, V. S. VEERASAMY, and W. I. MILNE: *Phys. Rev. Lett*., 1997, **78**, 4869.
84. K. W. R. GILKES, H. S. SANDS, D. N. BATHCHELDER, J. ROBERTSON, and W. I. MILNE: *Appl. Phys. Lett*., 1997, **70**, 1980.
85. V. PAJCINI, C. H. MUNRO, R. W. BORMETT, R. E. WITKOWSKI, and S. A. ASHER: *Appl. Spectrosc*., 1997, **51**, 81–86.
86. D. J. H. COCKAYNE and D. R. McKENZIE: *Acta Crystallogr. A*, 1988, **A44**, 870.

87. D. F. R. MILDNER and J. M. CARPENTER: *J. Non-Cryst. Solids*, 1982, **47**, 391–402.
88. F. LI and J. S. LANNIN: *Phys. Rev. Lett*., 1991, **65**, 1905.
89. D. C. GREEN, D. R. McKENZIE, and P. B. LUKINS: *Mater. Sci. Forum*, 1990, **52–53**, 103.
90. J. E. FIELD: 'Properties of diamond'; 1979, London, Academic Press.
91. Q. WEI: 'Structure and properties of *in situ* self-reinforced bulk Si_3N_4 ceramics and thin film diamondlike carbon prepared by pulsed laser deposition', PhD thesis, North Carolina State University, Raleigh, NC, USA, 1998.
92. Th. FRAUENHEIM, P. BLAUDECH, U. STEPHAN, and G. JUNGNICKEL: *Phys. Rev. B*, 1993, **B48**, 4823.
93. A. F. MYERS, E. B. STEEL, M. Q. DING, S. M. CAMPHSUSEN, W. B. CHOI, J. J. CUOMO, and J. J. HREN: in 'Covalently bonded disordered thin-film materials', (ed. M. P. Siegal *et al*.), Symp. Proc. 498, 83; 1998, Warrendale, PA, MRS.
94. S. CHRISTIANSEN, M. ALBRECHT, G. FRANK, H. P. STRUNK, C. RONNING, H. HOFSASS, and E. RECKNAGEL: *Diam. Relat. Mater*., 1998, **7**, 15–22.
95. F. XIONG, Y. Y. WANG, V. LEPPERT, and R. P. H. CHANG: *J. Mater. Res*., 1993, **8**, 2265–2272.
96. W. SCHARFF, K. HAMMER, O. STEUZEL, J. ULLMAN, M. VOGEL, T. FRAUENHEIM, B. EIBISCH, S. ROTH, S. SCHULZE, and I. MUHLING: *Thin Solid Films*, 1989, **171**, 157–169.
97. S. D. BERGER, D. R. McKENZIE, and P. J. MARTIN: *Philos. Mag. Lett*., 1988, **57**, 285–290.
98. H. RAETHER: in 'Springer tracts in modern physics', Vol. 88, 'Excitation of plasmon and interband transitions by electrons'; 1980, New York, Springer.
99. D. R. McKENZIE, R. C. McPHEDRAN, N. SAVVIDES, and L. C. BOTTEN: *Philos. Mag. B*, 1983, **B48**, 341.
100. J. BRULEY, L. M. BROWN, and S. D. BERGER: in 'Electron microscopy and analysis 1985', Conf. Proc. 78, 561; 1985, London, The Institute of Physics.
101. Z. L. AKKERMAN, H. EFSTATHIADIS, and F. W. SMITH: *J. Appl. Phys*., 1996, **80**, 3068.
102. T. SATO: *Jpn J. Appl. Phys*., 1967, **6**, 339.
103. N. M. RAVINDRA, S. ABEDRABBO, W. CHEN, F. M. TONG, A. K. NANDA, and A. C. SPERANZA: *IEEE Trans. Semicond. Manuf*., 1998, **11**, 30–39.
104. Q. WEI, J. SANKAR, A. K. SHARMA, R. J. NARAYAN, N. M. RAVINDRA, S. OKTYABRSKY, J. NARAYAN, and R. J. NARAYAN: *J. Mater. Res*., 2000, **15**, 633–641.
105. J. SCHÄFER, J. RISTEIN, R. GRAUPNER, L. LEY, U. STEPHAN, Th. FRAUENHEIM, V. S. VEERASAMY, G. A. J. AMARATUNGA, M. WEILER, and H. EHRHARDT: *Phys. Rev. B*, 1996, **B53**, 7762.
106. C. KITTEL: 'Introduction to solid state physics', 6th edn; 1986, New York, John Wiley.
107. C. A. DAVIS, K. M. KNOWLES, and G. A. J. AMARATUNGA: *Surf. Coat. Technol*., 1995, **76–77**, 316–321.
108. Y. YIN and D. R. McKENZIE: *Thin Solid Films*, 1996, **280**, 95–100.
109. R. GRAUPNER, J. RISTEIN, and L. LEY: *Surf. Sci*., 1994, **320**, 210.
110. K. C. PANDEY: *Phys. Rev. Lett*., 1982, **49**, 223.
111. D. W. BRENNER: *Phys. Rev. B*, 1990, **B42**, (15), 9458–9471.
112. J. ROBERTSON: *Diam. Relat. Mater*., 1997, **6**, 212.
113. G. GALLI, R. M. MARTIN, R. CAR, and M. PARINELLO: *Phys. Rev. Lett*., 1989, **62**, 555.
114. C. H. LEE, W. R. L. LAMBRECHT, and B. SEGALL: *Phys. Rev. B*, 1994, **B49**, 11448.
115. U. STEPHAN, Th. FRAUENHEIM, P. BLAUDECK, and G. JUNGNICKEL: *Phys. Rev. B*, 1994, **B49**, 1489.
116. D. A. DRABOLD, P. A. FEDDERA, and M. P. GRUMBACH: *Phys. Rev. B*, 1996, **B54**, 5480.
117. J. P. SULLIVAN and T. A. FRIEDMANN: in 'Amorphous carbon: state of the art', (ed. S. R. P. Silva *et al*.); 1998, Singapore,World Scientific.
118. K. SHIMATAWA and T. KAMEYAMA: *J. Non-Cryst. Solids*, 1989, **114**, 786.
119. A. BOZHKO, A. IVANOV, M. BERRETTONI, S. CHUDINOV, S. STIZZA, V. DORFMAN, and B. PYPKIN: *Diam. Relat. Mater*., 1995, **4**, 488.
120. G. A. J. AMARATUNGA, V. S. VEERASAMY, W. I. MILNE, C. A. DAVIS, S. R. SILVA, and N. S. MacKENZIE: *Appl. Phys. Lett*., 1993, **63**, 370.
121. R. ROBERTSON, J. ROBERTSON, and G. A. AMARATUNGA: *J. Appl. Phys*., 1996, **80**, 2998.
122. Q. LI, R. FANG, and Y. MA: *Thin Solid Films*, 1993, **226**, 99–103.
123. A. GRILL, V. PATEL, and C. JAHNES: *J. Electrochem. Soc*., 1998, **145**, 1649–1653.
124. J. P. SULIVAN, T. A. FRIEDMANN, C. A. APBLETT, M. P. SIEGAL, N. MISSERT, M. L. LOVEJOY, P. B. MIRKARIMI, and K. F. McCARTY: in 'Low-dielectric constant materials – synthesis and applications in microelectronics', Symp. Proc. 381, 273–278; 1995, Warrendale, PA, MRS
125. G. A. J. AMARATUNGA, J. ROBERTSON, V. S. VEERASAMY, W. I. MILNE, and D. R. McKENZIE: *Diam. Relat. Mater*., 1995, **4**, 637–640.
126. V. S. VEERASAMY, G. A. J. AMARATUNGA, C. A. DAVIS, W. I. MILNE, P. HEWITT, and M. WEILER: *Solid State Electron*., 1994, **37**, 319.
127. D. R. McKENZIE, Y. YIN, N. A. MARKS, C. A. DAVIS, B. A. PAILTHORPE, G. A. J. AMARATUNGA, and V. S. VEERASAMY: *Diam. Relat. Mater*., 1994, **3**, 353.
128. Z. Y. CHEN, Y. H. YU, J. P. ZHAO, X. WANG, S. Q. YANG, T. S. SHI, X. H. LIU, S. P. WONG, I. H. WILSON, J. B. XU, and E. Z. LUO: *Diam. Relat. Mater*., 1998, **7**, 491–494.
129. P. K. SITCH, Th. KOHLER, G. JUNGNICKEL, D. POROZAG, and Th. FRAUENHEIM: *Solid State Comm*., 1998, **100**, 549–553.
130. P. STUMM, D. A. DRABOLD, and P. A. FEDDERS: *J. Appl. Phys*., 1997, **81**, 1289–1295.
131. R. A. STREET: 'Hydrogenated amorphous silicon'; 1990, Cambridge, Cambridge University Press.
132. D. A. DRABOLD, P. STUMM, and P. A. FEDDERS: *Phys. Rev. Lett*., 1994, **72**, 2666.
133. C. A. DAVIS, Y. YIN, D. R. McKENZIE, L. E. HALL, E. KRAVTCHINSKAIA, V. KEAST, G. A. J. AMARATUNGA, and V. S. VEERASAMY: *J. Non-Cryst. Solids*, 1994, **170**, 46.
134. O. AMIR and R. KALISH: *J. Appl. Phys*., 1991, **70**, 4958.
135. O. STENZEL, M. VOGEL, S. PONITZ, R. PETRICH, T. WALLENDORF, C. V. BORCZYSKOWSKI, F. ROZPLOCH, Z. KRASILNIK, and N. KALUGIN: *Phys. Status Solidi A*, 1993, **A140**, 179.
136. C. RONNING, U. GRIESMEIER, M. GROSS, H. C. HOFSASS, R. G. DOWNING, and G. P. LAMAZE: *Diam. Relat. Mater*., 1995, **4**, 666.
137. A. HOLMBOLD, P. HAMMER, J. U. THIELE, K. ROHWER, and D. MEISSNER: *Philos. Mag. B*, 1995, **B72**, 335.
138. A. MANSOUR and D. UGOLINI: *Phys. Rev. B*, 1993, **B47**, 1020.
139. V. S. VEERASAMY, J. YUAN, G. A. J. AMARATUNGA, W. I. MILNE, K. W. R. GILKES, M. WEILER, and L. M. BROWN: *Phys. Rev. B*, 1993, **B48**, 17954.
140. D. DASGUPTA, F. DEMICHELIS, and A. TAGLIAFERRO: *Philos. Mag. B*, 1991, **B63**, 1255.
141. J. ROBERTSON: *Thin Solid Films*, 1997, **296**, 61–65.
142. B. F. COLL, J. E. JASKIE, J. L. MARKHAM, E. P. MENU, A. A. TALIN, and P. VON ALLMEN: in 'Covalently bonded disordered thin-film materials', Symp. Proc. 498, 185–196; 1998, Warrendale, PA, MRS.
143. J. ROBERTSON and M. J. RUTTER: *Diam. Relat. Mater*., 1998, **7**, 620–625.
144. S. R. P. SILVA and R. G. FORBES: *Ultramicroscopy*, 1998, **73**, 51–57.
145. J. ROBERTSON: in 'Covalently bonded disordered thin-film materials', Symp. Proc. 498, 197–208; 1998, Warrendale, PA, MRS.
146. X. LI, D. DIAO, and B. BHUSHAN: *Acta. Mater*., 1997, **45**, 4453–4461.
147. M. WEILER, S. SATTEL, T. GIESSEN, K. JUNG, and H. EHRHARDT: *Phys. Rev. B*, 1996, **B53**, 1594.
148. J. P. SULLIVAN, T. A. FRIEDMANN, and A. G. BACA: *J. Electron. Mater*., 1997, **26**, 1021.
149. J. SCHULTZ and M. NARDIN: in 'Handbook of adhesion science and technology', (ed. D. E. Packhaw); 1992, New York, John Wiley.
150. K. W. ALLEN: Proc. 10th Annual Meeting of The Adhesion Society Inc., Williamsburgh, VA, USA, February 1987.
151. A. ANTILA, J. SALO, and R. LAPPALAINEN: *Mater. Lett*., 1995, **24**, 153.
152. K. L. CHOPRA: 'Thin film phenomena'; 1969, New York, McGraw-Hill.
153. J. NARAYAN, S. SHARAN, and K. JAGANNADHAM: *J. Phys. (Paris)*, 1988, (Colloq. C5), 731.
154. S. B. IYER, K. S. HARSHAVADHAN, and V. KUMAR: *Thin Solid Films*, 1995, **256**, 94–100.
155. E. H. A. DEKEMPENEER, R. JACOBS, J. SMEETS, J. MENEVER, L. EERSELS, B. BLANPAIN, J. ROOS, and D. J. OOSTRA: *Thin Solid Films*, 1992, **217**, 51–56.
156. C. GALIOTIS: *Mater. Technol*., 1993, **8**, (9–10), 203–209.
157. L. S. SCHADLER and C. GALIOTIS: *Int. Mater. Rev*., 1995, **40**, (3), 116–134.
158. J. W. AGER III, S. ANDERS, A. ANDERS, and I. G. BROWN: *Appl. Phys. Lett*., 1995, **66** (25), 3444–3446.
159. Q. WEI, R. J. NARAYAN, A. K. SHARMA, J. SANKAR, and J. NARAYAN: in 'Covalently bonded disordered thin-film materials', Symp. Proc. 498, 61–66; 1998, Warrendale, PA, MRS.

160. Q. WEI, R. J. NARAYAN, J. NARAYAN, J. SANKAR, and A. K. SHARMA: *Mater. Sci. Eng*., 1998, **B53**, 262–266.
161. Q. WEI, R. J. NARAYAN, A. K. SHARMA, J. SANAKR, S. OKTYABRSKY, and J. NARAYAN: in 'Processing and properties of vapor deposited coatings', Symp. Proc. 555, 303–308; 1999, Warrendale, PA, MRS.
162. Q. WEI, R. J. NARAYAN, A. K. SHARMA, J. SANKAR, and J. NARAYAN: in 'Thin films: stresses and mechanical properties VII', Symp. Proc. 505, 331–336; 1998, Warrendale, PA, MRS.
163. Q. WEI, R. J. NARAYAN, A. K. SHARMA, J. SANKAR, and J. NARAYAN: *J. Vac. Sci. Technol. A*, 1999, **A17**, 3406–3414.
164. T. A. FRIEDMANN, J. P. SULLIVAN, J. A. KNAPP, D. R. TALLANT, D. M. FOLLSTAEDT, D. L. MEDLIN, and P. B. MIRKARIMI: *Appl. Phys. Lett*., 1997, **71**, (26), 3820–3822.
165. S. ANDERS, J. DIAZ, J. W. AGER III, R. Y. LO, and D. BOGY: *Appl. Phys. Lett*., 1997, **71**, 3367–3369.
166. A. C. FERRARI, B. KLEINSORGE, N. A. MORRISON, A. HART, V. STOLOJAN, and J. ROBERTSON: *J. Appl. Phys*., 1999, **85**, (10), 7191–7197.
167. O. R. MONTEIRO, M. P. DELPANCKE-OGLETREE, I. G. BROWN, and J. W. AGER III: in 'Materials modification and synthesis by ion beam processing', Symp. Proc. 438, 599–604; 1997, Warrendale, PA, MRS.
168. V. F. DORFMAN: *Thin Solid Films*, 1992, **212**, 267–273.
169. M. CRISCHKE, K. BEWILOGUA, K. TROJAN, and G. DIMIGEN: *Surf. Coat. Technol*., 1995, **74–75**, 739–745.
170. M. O. BENTZON, K. MOGENSEN, J. B. HANSEN, B. B. HANSEN, C. TAHOLT, P. HOLIDAY, and S. S. ESKILDSEN: *Surf. Coat. Technol*., 1994, **68–69**, 651–655.
171. M. ECKEL, G. KAMPSCHULTE, and P. MARKSCHLAGER: *Surf. Coat. Technol*., 1995, **74–75**, 827–832.
172. J. KOSKINEN, H. RONKAINEN, J.-P. HIRVONEN, R. LAPPALAINEN, and K. A. PISCHOW: *Diam. Relat. Mater*., 1995, **4**, 843–847.
173. C. DUMKUM, D. M. GRANT, and I. R. McCOLL: *Diam. Relat. Mater*., 1997, **6**, 802–806.
174. E. I. MELETIS, A. ERDEMIR, and G. R. FENSKE: *Surf. Coat. Technol*., 1995, **73**, 39–45.
175. J. DENG and M. BRAUN: *Diam. Relat. Mater*., 1995, **4**, 936–943.
176. A. A. VOEVODIN and J. S. ZABINSKI: *Diam. Relat. Mater*., 1998, **7**, 463–467.
177. A. A. VOEVODIN, M. A. CAPANO, S. J. P. LAUBE, M. S. DONELY, and J. S. ZABINSKI: *Thin Solid Films*, 1997, **298**, 107.
178. A. A. VOEVODIN, S. D. WALCK, and J. S. ZABINSKI: *Wear*, 1997, **203–204**, 516.
179. J. P. HIRVONEN, J. KOSKINEN, J. R. JERVIS, and M. NASTASI: *Surf. Coat. Technol*., 1995, **80**, 139–150.
180. R. LAPPALAINEN, H. HEINONEN, A. ANTILA, and S. SANTAVIRTA: *Diam. Relat. Mater*., 1998, **7**, 482–485.
181. A. A. VOEVODIN, M. S. DONLEY, J. S. ZABINSKI, and J. E. BULTMAN: *Surf. Coat. Technol*., 1995, **76–77**, 534–539.
182. S. T. PATTON and B. BHUSHAN: *IEEE Trans. Magn*., 1998, **34**, 575–587.
183. R. J. NARAYAN, Q. WEI, A. K. SHARMA, K. JAGANNADHAM, and J. NARAYAN: in 'Hard coatings based on borides, carbides and nitrides: synthesis, characterization and application', 301–308; 1998, Warrendale, PA, TMS.
184. E. MAROTTA, N. BAKHRU, A. GRILL, V. PATEL, and B. MEYERSON: *Thin Solid Films*, 1991, **206**, 188–191.
185. E. G. GERSTNER and D. R. McKENZIE: *Diam. Relat. Mater*., 1998, **7**, 1172–1177.